frontiers in Earth Science

ORIGINAL RESEARCH
published: 19 June 2020
doi: 10.3389/feart.2020.00223

Insights Into the Eruptive Dynamics of Small Caldera-Forming Eruptions: The Case Study of the Welded Scoriae of Vulcano (Aeolian Islands, Italy)

Eugenio Nicotra, Marta Minniti, Paola Donato and Rosanna De Rosa*

Dipartimento di Biologia, Ecologia e Scienze della Terra, University of Calabria, Cosenza, Italy

A multi-disciplinary study, integrating volcanological field observations, petrography, whole rock geochemistry and textural and compositional analyses on plagioclase crystals has been carried out on the products of Monte Luccia, Spiaggia Lunga, and Quadrara eruptions, occurred between 48 and 21 kyrs on the island of Vulcano. These products are all characterized by welded scoria blankets, and their eruptions have been generally related to the formation and/or re-activation of ring faults bordering the "Il Piano" caldera. The aim of the work is to reconstruct the pre- and syn-eruptive dynamics acting within their magma plumbing systems and the related link with the phases of caldera collapse. At the bottom of the stratigraphic sequences, the presence of base surge deposits suggests that all the eruptions started with a phreatomagmatic phase fed by a shallow reservoir. Textural and microanalytical study of plagioclase crystals of Spiaggia Lunga eruption revealed that the phreatomagmatic event activated the ascent of a volatile-rich, basaltic magma residing at 5–11 km of depth. This basaltic magma mixed with the resident shallow one, and was poured out during the course of the eruption producing a sustained lava-fountaining phase. The subsequent caldera collapse, identified by a layer of chaotic breccia interbedded in the scoriae deposit, has been linked to the partial emptying of the shallow magma reservoir. In contrast to what observed for recent eruptive events at Vulcano, the onset of the magmatic phase would be attributed to a self-activation due to volcano-tectonic events, and not to a pressurization of the plumbing system related to the ascent of deep magma batches. As concerns the Mt. Luccia deposits, bordering the eastern rim of the "Il Piano" caldera, the absence of plagioclase in the mineralogical assemblage suggests the eruption of a deeper magma (>11 km b.s.l.), rapidly ascending through the re-activated ring faults of "Il Piano" caldera. At Quadrara eruption, the occurrence of a layer of white biotite-bearing latitic pumices overlying the basal phreatomagmatic deposits suggests the involvement a shallow, isolated reservoir where the increase of volatile pressure allowed the crystallization of hydrous phases. A deeper shoshonitic magma was involved later in the eruption, forming the welded scoria level at the top of the sequence.

Keywords: caldera, plagioclase, magma plumbing system, eruptive scenario, pre-eruptive conditions, welded scoriae, volcanology, eruptive conditions

OPEN ACCESS

Edited by:
Marc-Antoine Longpré, Queens College (CUNY), United States

Reviewed by:
Andrea Di Muro, UMR 7154 Institut de Physique du Globe de Paris (IPGP), France
Jason Peter Coumans, Durham University, United Kingdom

****Correspondence:***
Eugenio Nicotra
eugenio.nicotra@unical.it

Specialty section:
This article was submitted to Petrology, a section of the journal Frontiers in Earth Science

Received: *28 February 2020*
Accepted: *27 May 2020*
Published: *19 June 2020*

Citation:
Nicotra E, Minniti M, Donato P and De Rosa R (2020) Insights Into the Eruptive Dynamics of Small Caldera-Forming Eruptions: The Case Study of the Welded Scoriae of Vulcano (Aeolian Islands, Italy). Front. Earth Sci. 8:223. doi: 10.3389/feart.2020.00223

INTRODUCTION

Calderas are one of the most evident morphological elements of a volcanic edifice. They differentiate from sector/flank-collapses or explosion craters, which could have similar aspect, chiefly for their direct link with the dynamics acting into the magmatic plumbing systems prior and during an eruptive event (e.g., Ventura et al., 1999; Peccerillo et al., 2007; Davì et al., 2009; Nicotra and Viccaro, 2012b; Fabbro et al., 2013; Fontaine et al., 2014; Kennedy et al., 2018; Albert et al., 2019). The processes promoting a caldera collapse are necessarily related to the presence of a magma reservoir, regardless of its shape, depth and composition. Collapses are chiefly related to magma displacement, which can produce a lateral intrusion or give rise to an eruption. The decrease of pressure within the reservoir can then lead to the collapse of its roof (Cashman and Giordano, 2014 for a review). Depending on the strength and thickness of the overlying country rock and on the width and depth of the magma chamber, caldera collapse can occur during syn- or post-eruptive phases of a single (or a sequence of) eruptive event(s). Usually this happens throughout some steps associated with seismic activity and/or minor aseismic creep subsidence events. Indeed, not all the caldera-forming processes are related to high-volume and catastrophic eruptive events, as the magnitude of the collapse is related to the ratio between the volume of the outpoured magmas and that of the magma chamber, and it is also function of the depth of the reservoir.

In most of geodynamic settings where magmatic processes develop through hundreds of thousands of years (e.g., continental rifting, collisional settings, back-arc extensional basin, complex geodynamic settings), magmas can pond and crystallize also at shallow depth, evolving toward silicic compositions (e.g., Davì et al., 2010; Peccerillo and Frezzotti, 2015; Andersen et al., 2017). The extreme evolution of such magmatic systems toward rhyolitic *s.l.* compositions, often leads to large-volume and high-energy caldera-forming eruptions (e.g., Jellinek and de Paolo, 2003; Cashman and Giordano, 2014). Despite the very low aspect ratio of mafic magma reservoirs, also the associated volcanic edifices can be affected by calderas. One of the best examples is represented by Etna volcano, which underwent repeated caldera-forming episodes at the ends of periods of huge magma withdrawal from its shallow reservoirs ["Il Piano" (15 kyrs), 122 b.C. eruption and 1669 eruption calderas; Coltelli et al., 1998; Nicotra and Viccaro, 2012b]. Other famous, and in some cases similar, examples are the Kilauea, Piton de la Fournaise and some volcanoes of Galapagos and Canary archipelagos (e.g., Fontaine et al., 2014; Harpp and Geist, 2018; Kennedy et al., 2018; Albert et al., 2019; Sainz-Maza Aparicio et al., 2019). Nonetheless, the mechanisms controlling the caldera formation at mafic systems, usually drawn as a sequence of melt lenses or stacked sills at different depths of the magmatic plumbing system (e.g., Marsh, 1996; Annen and Sparks, 2006; Gudmundsson, 2012; Nicotra et al., 2018), are still poorly understood.

Within the last 130 kyrs of its volcanic activity, the morphology of the island of Vulcano deeply changed due to several caldera-forming stages, finally leading to the formation of the two calderas of "Il Piano" and "La Fossa" (**Figure 1**). In particular, the re-activation of the "Il Piano" caldera is usually associated to some small-volume, but highly energetic, eruptions developed between 48 and 21 kyrs on its caldera rims (i.e., Monte Luccia, Spiaggia Lunga, Quadrara Formations; **Figure 1**). The most voluminous (ca. 0.1 km^3) and best preserved of them is certainly that of Spiaggia Lunga (**Figures 1**, **2**; ca. 24 kyrs; Soligo et al., 2000). One of the most intriguing features of these eruptions is the similarity of their products, having all erupted massive reddish and strongly welded scoriae with a shoshonitic affinity. Similar volcanic deposits have been also successively erupted later on at Monte Saraceno, on the southern border of the caldera of "La Fossa" (ca. 8 kyrs; De Astis et al., 2013). The welded scoriae of Vulcano, especially those of Spiaggia Lunga, have been subject to different interpretations of their eruptive mechanisms, being considered as trachybasaltic ignimbrites (Keller, 1980; Gioncada and Sbrana, 1991) or, alternatively, as the products of a strong Strombolian activity, forming a clastogenic lava flow on the western slope of the island (**Figure 1**; De Rosa et al., 1988; De Astis et al., 2013). According to both interpretations, the strong welding of the deposits gives them a "lava-like" aspect. However, despite the great similarity of the Monte Luccia, Spiaggia Lunga, and Quadrara deposits and the similar topographic position along the ring faults of the caldera of "Il Piano," the possible relationship between these eruptive events and the episode of caldera formation has not been analyzed in detail.

The present study is focused on the reconstruction of the pre- and syn-eruptive magma dynamics acting into the plumbing systems of these eruptions, their eruptive scenarios and possible role in triggering episodes of caldera collapse. These purposes have been pursued by means of multi-disciplinary studies joining the volcanological field survey with petrographic observations, textural and compositional (EMPA) studies on plagioclase crystals and whole rock compositions (XRF).

VOLCANOLOGICAL BACKGROUND

The Island of Vulcano

Vulcano is the southernmost island of the Aeolian archipelago, a volcanic arc located between the back-arc oceanic basin of Marsili and the continental foreland Calabrian arc. Aeolian islands are the result of the subduction of the Mesozoic Ionian slab beneath the Calabrian arc, as testified by the presence of a NW-dipping Benioff zone under the arc (e.g., Barberi et al., 1974; Gasparini et al., 1982; Ellam et al., 1989). Seismicity observed in this area is attributed to the passive subduction and de-hydration of a detached slab, which would be also the cause of the Aeolian volcanism in a context of post-subduction extensional tectonic regime (Wang et al., 1989; Crisci et al., 1991; Esperança et al., 1992; Gvirtzman and Nur, 1999). The islands of Vulcano, Lipari and Salina, in the central portion of the archipelago, are affected by NNW–SSE-striking faults (Tindari–Letojanni Fault System; cf. Barberi et al., 1994; Ventura, 2013) and are located above a 15–20 km thick continental crust (De Ritis et al., 2013) consisting of the Hercynian metamorphic and granitic rocks and Mesozoic sediments of the Calabrian basement (Keller, 1980; Del Moro et al., 1998; Frezzotti et al., 2004).

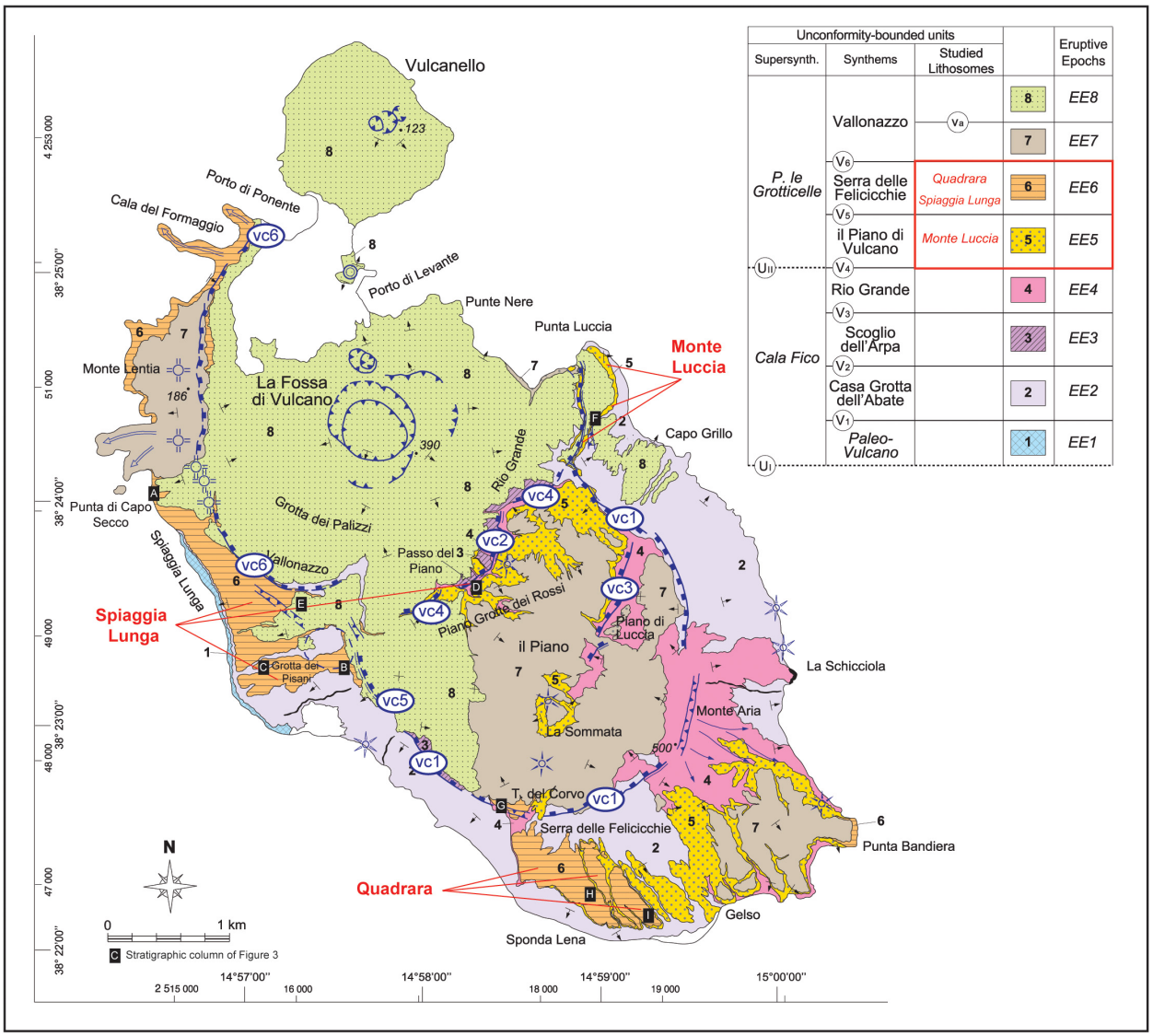

FIGURE 1 | Geological sketch map of the island of Vulcano (from De Astis et al., 2013). The studied areas of Monte Luccia, Spiaggia Lunga and Quadrara are indicated. vc = volcano-tectonic collapse. White letters in black box are referred to the stratigraphic columns of **Figure 5**.

The subaerial portion of the island of Vulcano is part of a wider complex including the islands of Lipari and Salina, developed along a graben-like structure controlled by the NNW-SSE strike-slip Tindari-Letojanni fault system (e.g., Ventura, 2013; Ruch et al., 2016). The subaerial activity at Vulcano covers the last 127 kyrs, and spatially shifted with time from south toward north. In the eruptive history of Vulcano De Astis et al. (2013) distinguished 8 Eruptive Epochs (EEs; cf. **Figure 1**) separated by 6 different volcano-tectonic (vc) collapses, which produced the multi-stage calderas of "Il Piano" and "La Fossa."

The first vc1 collapse occurred at about 100 kyrs during the EE3 and produced the main depression of the "Il Piano" caldera (**Figure 1**). It was followed by the vc2 collapse, which formed the southern border of the younger "La Fossa" caldera. The vc3 collapse was internal to the "Il Piano" caldera, in the area of Piano di Luccia (**Figure 1**), and it is supposed to have formed between 70 and 42 kyrs. While vc4 and vc6 collapses were related to the "La Fossa" caldera, the vc5 collapse is a tardive volcano-tectonic vertical movement occurred (probably) between 24 and 21 kyrs and reactivating the western rim of "Il Piano" caldera (**Figure 1**; De Astis et al., 2013).

The Welded-Scoriae Enigma

The present work focuses on blankets of mafic-intermediate welded scoriae outcropping in different areas of the island of Vulcano dated between 48 and 21 kyrs (**Figures 1–4**), whose relationships and stratigraphic position has been a matter of debate during the last 40 years, mainly due to the lack of certainty in absolute dating. Following De Astis et al. (2013) we will adopt the "classical" names of these deposits, related to the locus of

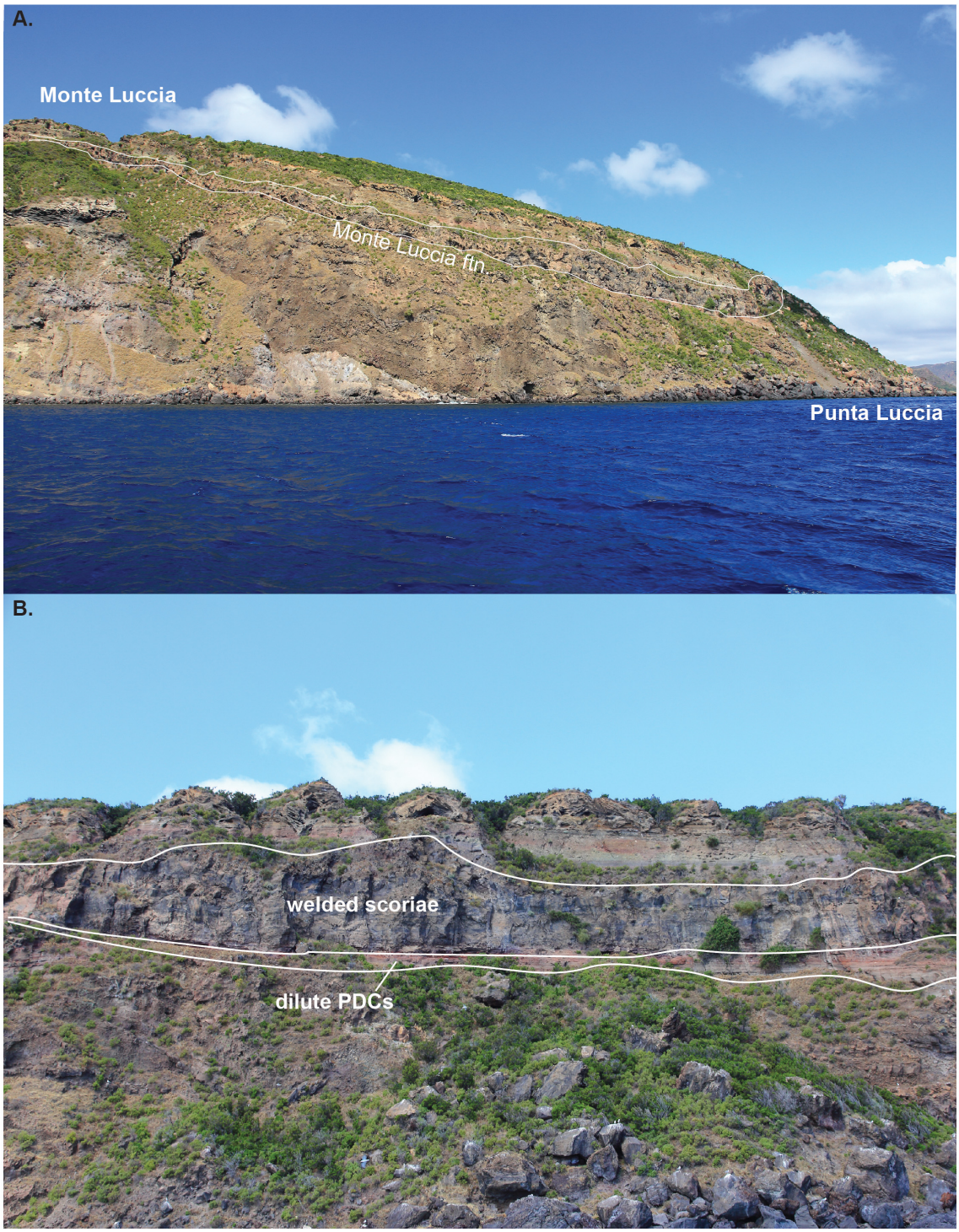

FIGURE 2 | Photos of Punta Luccia area, along the northern coasts of Vulcano island. **(A)** Panorama of the Monte Luccia formation; here the welded scoriae reach 25 m of thickness. **(B)** Detail photo of the Monte Luccia Formation, with indication of the dilute PDCs deposits at its base.

the best-preserved stratigraphy, i.e., Monte Luccia (ML), Spiaggia Lunga (SL), and Quadrara (Qu) formations. Before and after these eruptive periods, other welded scoriae have been erupted at Vulcano island (e.g., Monte Aria, Passo del Piano, La Sommata, Monte Saraceno; cf. De Astis et al., 2013); however, each of these eruptive events presents different and peculiar features and compositions with respect to the more homogeneous ML-SL-Qu sequences.

FIGURE 3 | Photos of various areas of Spiaggia Lunga deposits. **(A)** Panoramic photos of the southern cliffs of Vulcano island; at its top the SL blanket, whose thickness increases from Capo Secco (south) to Punta di Capo Secco (north). **(B)** Particular of SL deposits. **(C)** "Lava-like" portion of the SL deposits. **(D)** Proximal area of SL deposits in a 10 m thick succession: it is possible to see the variation of welding from distal (left) to more proximal (right) portions of the deposit. **(E)** Particular of the base of the succession of SL deposits at Punta di Capo Secco. A metric block produced a bomb sag on the soft cross-laminated underlying deposits of dilute PDCs. **(F)** Proximal area of SL Formation, at the top of Monte Saraceno: the two different portions of the outcrops, with different degree of welding, are very evident. At the top, Saraceno ftn. Is overlying with angular unconformity. **(G)** Lower portion of the deposits of SL in the same location of **(F)**. It is still possible to recognize an agglutinated spatter block.

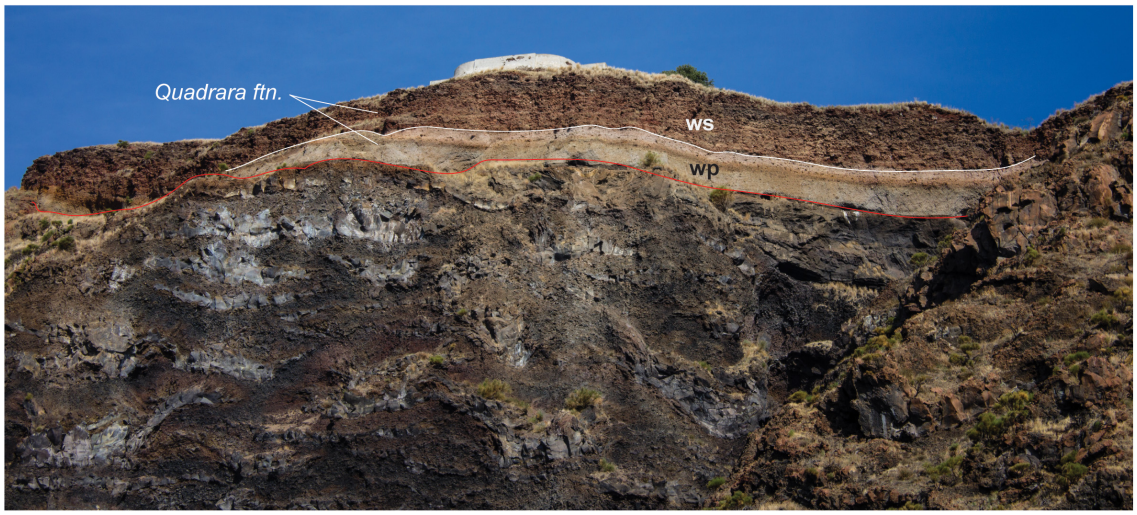

FIGURE 4 | Panoramic view of the Quadrara Formation, in the southernmost area of Vulcano island. Deposit can be divided into the wp (white pumices) and WS (welded scoriae) portions.

Keller (1980) defined blankets of welded scoriae the pyroclastic deposits outcropping at Monte Luccia, Spiaggia Lunga, and Quadrara areas, and considered all of them in the same stratigraphic position. He described these products as "lava-like banks" covering a pre-existing morphology which, toward their marginal and top portions, turn in deposits with coarse eutaxitic "fiamme" structures and then in less agglutinated scoriae and bombs. Keller (1980) interpreted these features as related to the deposition of trachybasaltic ignimbrites, with gas-rich magma erupted as hot pyroclastic flow during the collapse of segments of the "Il Piano" caldera. Such interpretation has been also embraced later by Gioncada and Sbrana (1991).

De Rosa et al. (1988), studying the SL welded scoriae (**Figure 2**), related these deposits to a low-energy fissure eruption along a segment of the "Il Piano" caldera. During the initial stages of the eruption magma interacted with external water, whereas at the climax a purely magmatic eruption led to the craterization of the fissure and very rapid drainage of the uprising magma.

The stratigraphic position of these formations has been discussed by De Astis et al. (1989), which gave an age of 48.5 ± 6.5 kyrs for ML deposits. The authors hypothesized also a stratigraphic continuity between the top of SL deposits and the base of Lentia dome (ca. 15 kyrs), linking them with two phases of collapse of the "La Fossa" caldera. According to De Astis et al. (1989) and in contrast with the Keller (1980) hypothesis, the ML-SL-Qu deposits would belong to three different eruptions and, therefore, occupy three different stratigraphic positions. Further U/Th absolute dating of Soligo et al. (2000) did not allow to definitively assess the different stratigraphic position for the Spiaggia Lunga (24.0 ± 5.0 kyrs) and Quadrara (21.3 ± 3.4 kyrs) Formations, due to the overlapping ages.

Recently, the ML welded deposits (**Figure 3**) have been attributed by De Astis et al. (2013) to Strombolian-Hawaiian explosive activity, coupled with a density-stratified scoria flow. This would be consistent with the lentiform geometry of the unit, its valley-ponding thickness variations, a well-developed foliation and the homogeneous SW-NE magnetic fabric found by Zanella et al. (2001). Furthermore, these authors recognized a lithic-rich horizon in the medial portion of the outcrop, and a cross-laminated tuff layer at the base of the unit, related to a short-lived phreatomagmatic phase that produced a sequence of discontinuous dilute PDCs. A similar deposit has been recognized also at the base of SL (**Figure 2E**; De Astis et al., 2013). Here, the activity continued with open-conduit-related, lithic-rich deposits and evolved into intense Strombolian explosive activity. Also in this case, a slight valley-ponding thickness variation, together with the homogeneous magnetic fabric and SE-NW magnetic lineation recognized by Zanella et al. (2001), led to the interpretation of SL deposits as due to a fountain-fed fallout coupled with scoria flow movements. De Astis et al. (2013) recognized for the first time an epiclastic breccia layer within the SL sequence. The same depositional mechanism has been also hypothesized for the Qu sequence (**Figure 4**), which at its base shows inversely graded biotite-bearing light pumices, gradually passing into a scoria blanket (De Astis et al., 2013), suggesting the progressive tapping of a zoned magma reservoir during the Quadrara eruption.

SAMPLING AND ANALYTICAL METHODS

A volcanological survey and a sampling campaign were carried out on all the deposits of welded scoriae belonging to the ML-SL-Qu Formations (**Figures 1–4**). As a whole, 43 representative rock samples were collected from 9 volcano-statigraphic columns (**Figure 5**).

Whole rock data for all the collected samples are reported in **Table 1**. Whole rock compositions in terms of major and some trace elements were obtained at the Dipartimento di Biologia, Ecologia e Scienze della Terra of the University

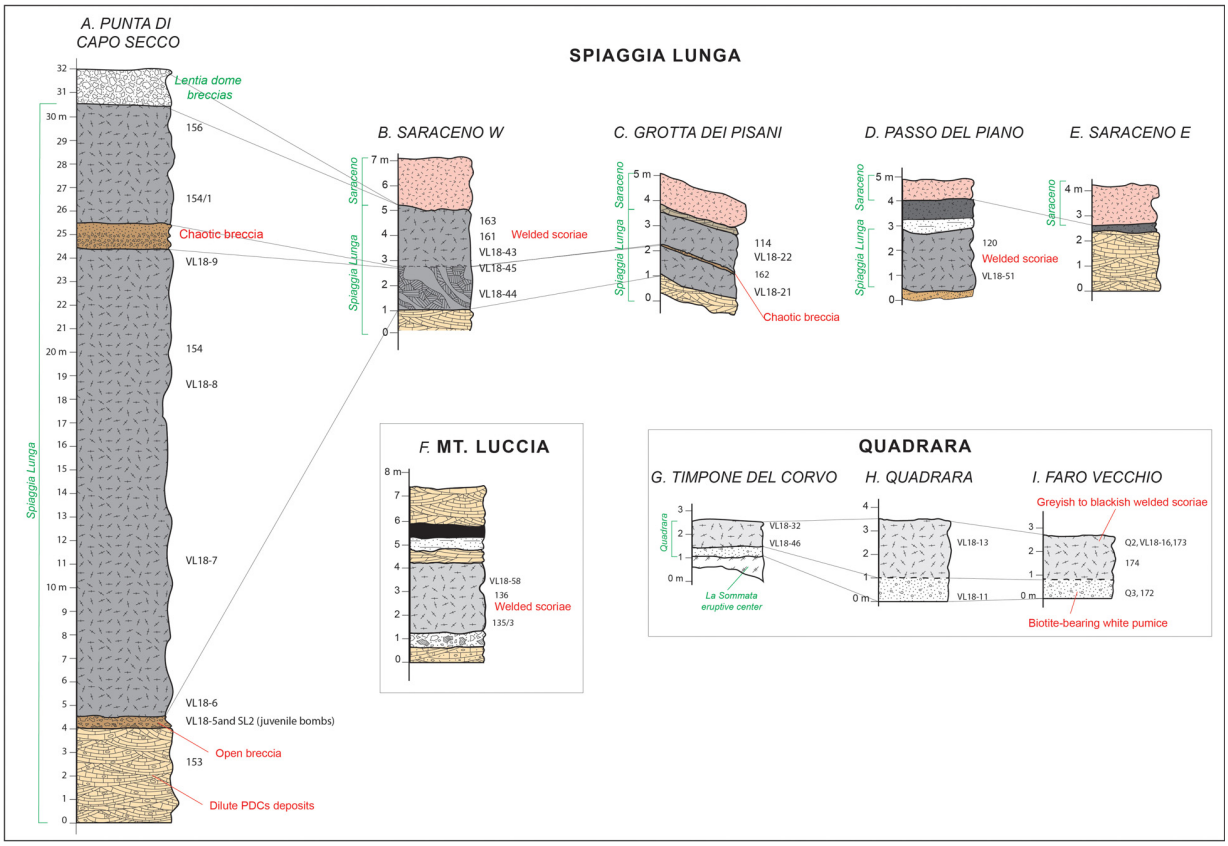

FIGURE 5 | Stratigraphic successions of the studied eruptive events. The location of each column is indicated by the capital white letter in the black box of **Figure 1**.

of Calabria (Italy) by means of a Bruker S8 Tiger XRF spectrometer on powder pellets with matrix effect corrections. The precision, measured as percentage difference between certified and measured composition of standards analyzed as unknown samples, was always <5% for major elements and 10% for trace elements. FeO was determined by titration. Loss on ignition was determined by gravimetric methods and corrected for Fe^{2+} oxidation. The sum of oxides was always higher than 98%. All the analyses were re-calculated for a sum of 100%.

On 25 selected rock samples, polished thin sections were obtained. Mineralogical and petrographic observations were performed by means of optical and polarized microscope. Compositional core-to-rim profiles were executed on 23 plagioclase crystals on polished, graphite-coated thin sections by means of Electron MicroProbe Analyzer (EMPA). Plagioclase crystals were selected on the basis of the representativeness of their texture within each sample. Only phenocrysts were considered for this type of analysis; in this regard, the plagioclase xenocrysts of Monte Luccia and the xenocrystic cores occurring in Spiaggia Lunga welded scoriae were not taken into account for textural and compositional analysis. All compositional data on plagioclase are reported in **Supplementary Material**. We used the JEOL JXA-8230 of SILA-CM2 lab at the University of Calabria, equipped with 5 WDS and one EDS spectrometers. WDS analyses were carried out with an accelerating voltage of 15 kV and probe current of 10 nA. Count times were of 15 s for Na and 30 s for other elements.

FIELD DATA

Monte Luccia Formation (ML)

Monte Luccia formation (48.5 ± 6.5 kyrs; De Astis et al., 1989) crops out on the northern and central portion of the island, where the rim of the "Il Piano" caldera is cut by that of the "La Fossa" (**Figure 1**). It consists of a pyroclastic succession with variable thickness from 3 m at the top of Monte Luccia up to 25 m at its base (**Figure 3**). Welded scoriae overlie a 0.5–1 m thick cross-laminated tuff layer (**Figure 3B**), generated by dilute PDCs, and by a level of altered breccia, whose thickness increases in the morphological depressions. The main portion of ML is made up by a blanket of reddish scoriaceous bombs, from very (at the base) to poorly welded (at its top). At the very top of the layer it is possible to distinguish each single lava spatter shred. The deposits are covered by the Grotta dei Palizzi Formation belonging to the "La Fossa" hystorical activity (cf. De Astis et al., 2013).

Spiaggia Lunga Formation (SL)

Among all the outcrops of welded scoriae at Vulcano island, those of the Spiaggia Lunga Formation (24.0 ± 5.0 kyrs;

TABLE 1 | Whole rock composition for the considered eruptive events.

Formation	Mt. Luccia	Mt. Luccia	Mt. Luccia	Spiaggia Lunga	Spiaggia Lunga	Spiaggia Lunga	Spiaggia Lunga	Spiaggia Lunga	Spiaggia Lunga	Spiaggia Lunga	Spiaggia Lunga	Spiaggia Lunga	Spiaggia Lunga	Spiaggia Lunga	Spiaggia Lunga
Type	**wd**	**wd**	**pdc**	**wd**	**wd**	**wd**	**wd**	**wd**	**scoriae**	**wd**	**wd**	**wd**	**wd**	**wd**	**wd**
Sample	**VL18_58**	**136**	**135/3**	**120**	**VL18_51**	**114**	**VL18_22**	**VL18_21**	**163**	**161**	**VL18_43**	**VL18_45**	**VL18_44**	**156**	**154/1**
SiO_2	52.8	52.0	50.5	49.8	50.3	50.9	51.2	52.0	48.6	51.3	52.4	53.2	54.0	48.3	48.3
TiO_2	0.68	0.72	0.84	0.84	0.78	0.69	0.77	0.80	0.86	0.67	0.65	0.69	0.71	0.68	0.70
Al_2O_3	17.0	19.0	16.4	19.8	18.4	18.7	19.3	16.6	18.6	20.3	21.6	18.5	17.9	22.1	19.6
Fe_2O_3	5.71	5.63	10.42	6.39	6.02	3.79	8.75	7.00	8.49	5.40	7.14	7.85	6.34	7.64	6.24
FeO	3.02	2.69	2.40	3.57	3.75	3.84	1.20	3.00	1.90	1.55	0.48	0.49	1.75	0.17	1.96
MnO	0.16	0.13	0.13	0.21	0.17	0.22	0.16	0.17	0.28	0.43	0.13	0.14	0.17	0.16	0.17
MgO	3.66	3.00	2.58	3.36	3.71	3.01	3.00	4.32	3.96	1.96	1.77	2.81	3.33	2.02	3.01
CaO	7.02	5.48	4.79	7.48	7.55	6.08	7.60	8.84	8.77	5.99	5.43	6.72	6.93	6.60	7.06
Na_2O	2.78	2.75	1.76	2.12	2.69	2.78	2.69	2.94	2.60	2.46	2.53	2.99	2.92	2.17	4.11
K_2O	3.51	3.65	2.59	2.76	2.74	2.87	2.78	2.93	2.44	3.07	3.45	3.33	3.21	3.22	2.67
P_2O_5	0.32	0.31	0.56	0.26	0.29	0.33	0.30	0.29	0.29	0.36	0.35	0.37	0.33	0.34	0.32
Ba	763	770	n.a.	785	776	851	801	831	786	997	887	892	903	740	722
Ce	122	85	n.a.	84	77	73	98	72	100	110	90	102	102	100	102
Co	42	n.a.	n.a.	n.a.	32	n.a.	36	37	n.a.	n.a.	16	23	26	n.a.	n.a.
Cr	67	51	n.a.	20	23	16	21	25	15	13	14	14	13	11	10
La	61	43	n.a.	47	48	44	45	37	43	49	52	59	67	42	43
Nb	15	12	n.a.	7	9	7	9	7	6	10	13	12	13	6	6
Ni	31	24	n.a.	20	22	41	14	22	22	37	17	22	18	16	22
Pb	20	n.a.	n.a.	n.a.	16	n.a.	12	19	n.a.	n.a.	9	15	15	n.a.	n.a.
Rb	104	111	n.a.	62	68	55	41	62	52	91	110	100	71	70	56
Sr	936	735	n.a.	1075	1131	1526	1134	1322	1282	958	943	1280	1153	969	1137
V	240	245	n.a.	277	280	297	231	292	292	117	113	163	214	209	223
Y	31	33	n.a.	56	36	29	40	19	29	45	46	24	28	69	31
Zr	123	122	n.a.	109	101	109	102	99	105	126	132	134	137	98	100

(Continued)

TABLE 1 | Continued

Formation	Spiaggia Lunga	Spiaggia Lunga	Spiaggia Lunga	Spiaggia Lunga	Spiaggia Lunga	Spiaggia Lunga	Spiaggia Lunga	Quadrara	Quadrara	Quadrara	Quadrara	Quadrara	Quadrara	Quadrara
Type	**wd**	**wd**	**wd**	**wd**	**wd**	**scoriae**	**Bomb**	**wd**	**wd**	**wd**	**wd**	**pumice**	**pumice**	**pumice**
Sample	**154**	**VL18_9**	**VL18_8**	**VL18_7**	**VL18_6**	**SL2**	**VL18_5**	**VL18_32**	**VL18_16**	**173**	**174**	**VL18_13**	**VL18_11**	**172**
SiO_2	50.2	50.3	51.6	51.4	51.7	50.9	50.3	53.4	54.5	55.5	55.8	59.0	59.5	59.9
TiO_2	0.71	0.78	0.74	0.75	0.74	0.88	0.82	0.77	0.82	0.82	0.79	0.55	0.46	0.52
Al_2O_3	19.0	17.9	17.9	18.4	17.7	17.0	16.8	16.6	16.7	17.5	17.6	17.3	18.8	18.1
Fe_2O_3	7.75	7.75	7.29	8.02	7.43	7.54	8.37	4.81	9.05	7.44	7.71	5.45	3.46	3.55
FeO	0.76	2.21	1.94	1.66	2.01	3.45	2.65	4.92	0.59	0.66	0.12	0.57	1.34	1.26
MnO	0.18	0.16	0.17	0.17	0.18	0.21	0.30	0.19	0.15	0.16	0.15	0.18	0.12	0.17
MgO	2.85	3.35	3.40	3.45	3.31	4.21	4.23	3.37	3.39	2.89	2.88	2.00	1.15	1.57
CaO	9.36	8.72	8.28	7.84	8.02	8.71	9.48	7.63	6.83	6.14	5.96	3.97	2.33	2.93
Na_2O	5.01	2.77	3.39	2.93	3.15	2.96	2.89	2.92	3.12	3.43	3.42	4.04	1.95	3.83
K_2O	2.74	2.77	2.88	2.73	3.09	2.99	2.84	4.37	3.81	4.31	4.42	5.05	3.49	5.11
P_2O_5	0.43	0.36	0.40	0.35	0.39	0.31	0.28	0.46	0.37	0.40	0.40	0.24	0.20	0.21
Ba	780	817	850	797	873	896	935	1123	910	929	934	1100	1069	n.a.
Ce	83	67	81	73	84	71	70	106	102	115	115	99	118	n.a.
Co	n.a.	28	30	32	34	34	42	34	26	n.a.	n.a.	9	4	n.a.
Cr	10	12	n.a.	16	14	19	17	n.a.	n.a.	0	0	n.a.	n.a.	n.a.
La	42	40	41	36	53	52	37	60	59	50	51	53	49	n.a.
Nb	6	11	10	9	6	6	9	20	14	12	13	20	21	n.a.
Ni	16	17	24	21	22	25	22	16	6	7	6	10	7	n.a.
Pb	n.a.	11	11	11	11	13	12	25	13	n.a.	n.a.	45	24	n.a.
Rb	27	26	24	31	57	59	69	129	106	132	133	167	134	n.a.
Sr	1178	1284	1310	1221	1348	1136	1431	1348	1245	1175	1156	1113	866	n.a.
V	191	264	243	273	265	349	293	268	187	158	144	78	63	n.a.
Y	27	30	28	25	29	26	26	26	26	27	29	35	30	n.a.
Zr	95	102	99	99	97	140	104	144	146	157	153	196	212	n.a.

Wd, welded scoriae. ***Supplementary Material*** *– Core-to-rim compositional profiles on 23 selected plagioclase crystals.*

Soligo et al., 2000) are the best preserved and most voluminous. The deposits of this eruption are widely distributed on the eastern parts of the island, following the shape of the eastern rims of the "Il Piano" and "La Fossa" calderas (**Figure 1**).

The most voluminous and best-preserved flow units are located at the intersection of these two caldera systems, in correspondence of the cliffs of "Punta di Capo Secco" (**Figures 1**, **2**, **5**). The base of this outcrop is constituted by 4 m of thickly bedded, planar to wavy and cross-laminated, thin (<10 cm) ash deposits (**Figures 2D,E**, **5**), carrying some lithics (up to 17–18 cm) and having bomb sags with a N110°E direction, that can be clearly attributed to a dilute PDC. These PDC deposits are typically characterized by a high frequency of thin layers rich in juvenile fragments and accretionary lapilli and of crustal xenoliths of leuco-monzogabbro (cf. Faraone et al., 1986) up-to-25 cm in size. Such features suggest that these PDC could have a phreatomagmatic origin, in which country rocks have been carried out at the surface together with the magmatic component. Toward the top, these deposits (**Figures 2E**, **5**) end with a 0.5 m thick layer very rich in brecciated lithics (crustal and volcanics) and juvenile bombs (up to 10 cm; **Figure 2E**) generating bomb-sags with a N110°E direction of provenance. Due to these features, this layer can be interpreted as an opening breccia.

The main portion of the SL is constituted by a 25 m thick massive layer made up by mildly welded to strongly welded or "lava-like," scoriaceous deposits (**Figures 2**, **5**). The degree of welding clearly varies with the thickness of the deposit. Following the cliff of this outcrop from "Punta di Capo Secco" to "Capo Secco" promontory (from north to south; **Figure 1**), the deposit changes progressively from "lava-like" (up to 25 m of thickness) to strongly welded in the intermediate portions (ca. 15 m of thickness) and finally to mildly or weakly welded where thickness is lower than 10 m. Vitric, elongated structures, interpreted by Keller (1980) as fiammae, were recognized in the basal and top portion of the deposit. Conversely, our field evidence suggests that "fiammae-like" structures found at the bottom and the top of SL are the agglutinated surfaces of each bomb, stretched and ripped off by the growing thickness of the deposit. In the upper part of "Punta di Capo Secco" outcrop, at about 5 m from the top, a 1 m thick deposit of fine and lithic-rich ash is interbedded in the welded scoriae of SL. It corresponds to the "epiclastic breccia layer" of De Astis et al. (2013), and it has been also found in the Grotta dei Pisani area (**Figures 1**, **5**), at highest elevation, where the dimensions of brecciated lithics are larger. At "Punta di Capo Secco" the succession is closed by the brecciated deposits of the Lentia domes (ca. 15 kyrs; De Rosa et al., 2003).

The SL deposits also crop out on the high western flank of Mt. Saraceno (**Figures 1**, **2F,G**), on a 25° steep slope. Here, above the cross-laminated PDCs deposits, two portions can be identified (**Figure 5**). The lowermost portion is constituted by a 1 m thick layer of mildly to strongly welded scoriae and bombs, where the single ballistic fragments can still be recognized (**Figure 2G**). The uppermost is a 5–8 m thick "lava-like" deposit very similar to those of "Punta di Capo Secco" (**Figure 2F**). The stratigraphic and topographic position, joined to the depositional features, lead to consider these deposits as proximal. These two layers are separated by a very thin (<1 cm) deposit of fine ash, also outcropping in the "Grotta dei Pisani" area (**Figure 5**), and corresponding to the inter-layered epiclastic breccia deposits recognized by De Astis et al. (2013) in the SL succession.

Quadrara Formation (Qu)

The Quadrara Formation (21.3 ± 3.4 kyrs; Soligo et al., 2000) crops out on the southernmost portion of the "Il Piano" caldera, mantling the outer border of the volcanic edifice (**Figures 1**, **4**). This Formation, related to a single eruptive event, starts with few centimeters of fine ash laminated beds rich in lithics followed by 1 m thick layer of inversely graded and biotite-bearing white pumices (**Figure 4**). Although at "Faro Vecchio" it seems that white pumices progressively grade into the overlying mildly to strongly welded blackish scoria deposit, at "Quadrara" and "Timpone del Corvo" areas a layer of very fine unsorted and ungraded ash separates the pumice layer from the upper scoria deposit (**Figure 5**).

WHOLE ROCK GEOCHEMISTRY

Whole rock geochemistry of the analyzed welded scoriae at Vulcano island confirms that all the products belong to the shoshonitic series, coherently with literature data for rocks of these eruptive epochs (Keller, 1980; De Astis et al., 1997; De Astis et al., 2013; Nicotra et al., 2018). On the whole (**Figure 6A**), the considered samples mainly plot into the shoshonitic basalt and shoshonite fields, with only the pumice of Qu and some samples of SL which show latitic composition.

It is worth of note that whole rock composition of samples of SL at Capo Secco (**Figures 1**, **2**, **5**) tends to be slightly less evolved from the base to the top of the succession (**Figure 6C** and **Table 1**). A significant variation is also shown by some trace elements, such as Ba and Nb, which, from the bottom to the top of the succession, decrease and increase, respectively. By contrast, the SL samples of the western flank of Mt. Saraceno (VL18-43/45/44; **Table 1**) show fairly constant compositions, similar to those of the deposits at the base of Capo Secco succession (K_2O = 3.2–3.4 wt%). Within the sequence of Quadrara, the white pumices at the base of the succession show the most evolved compositions, being classified as latite (**Figure 6A**). Conversely, in the dark scoriae above the cm-thick epiclastic layer, whole rock compositions tend to be gradually more basic. The diluted PdC deposit at the base of Monte Luccia is slightly less evolved and Ca-rich than the overlying scoriae (**Figures 6A,B**).

Spider diagram normalized to Primordial Mantle (**Figure 6D**) shows a superimposition of the patterns of all the samples, with only the Quadrara latites slightly more enriched in Rb, Ba, Nb, K, Zr, and depleted in P and Ti.

PETROGRAPHY AND MINERAL CHEMISTRY

Petrographic analysis has been carried out on most representative samples of the considered formations, including also the dilute

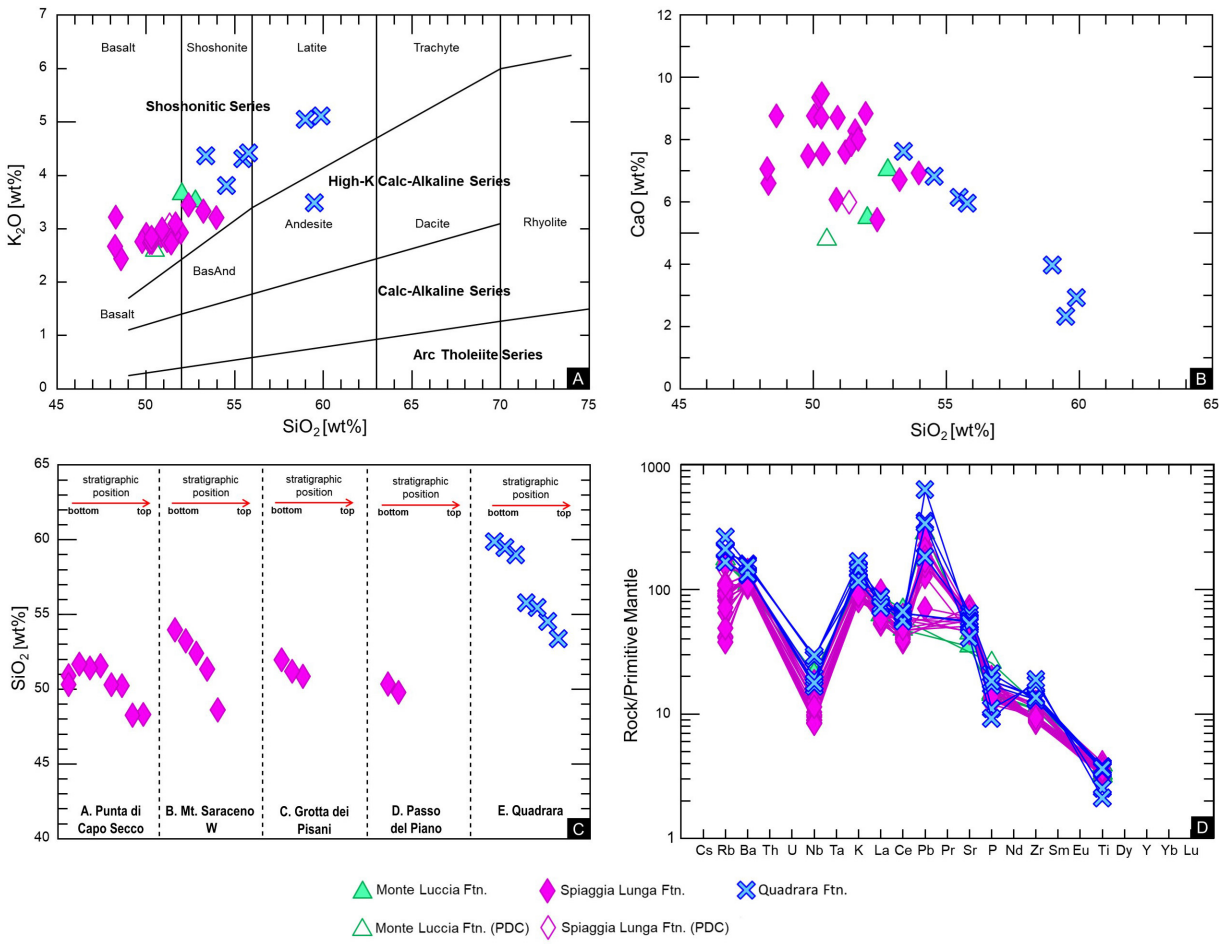

FIGURE 6 | Whole rock diagrams for the collected rock samples. **(A)** Peccerillo and Taylor (1976) classificative diagram; **(B)** CaO vs. SiO_2 variation; **(C)** variation of SiO_2 content with stratigraphic height in the different sampled outcrops; **(D)** primordial mantle- normalized (Sun and McDonough, 1989) spider diagram of incompatible elements contents.

PDCs and pumice samples which preceded the emplacement of welded scoriae.

One of the most intriguing features is that the most welded part of each formation, especially in the central portion of SL, exhibits a "lava-like" texture also at microscopic scale. Less welded deposits have a more scoriaceous structure, often characterized by the unique presence of rapidly chilled and highly vesiculated glass. Although characterized by a strong vesiculation due to syn- and post-eruptive degassing, the most welded deposits generally have a porphyritic structure, with a variable porphyritic index (P.I. in vol%) that ranges from 5 to 45% (ML = 10–15%; SL = 35–45%; Qu = 5–15%). Groundmass varies from hypo-crystalline to aphanitic and from micro- to crypto-crystalline; it is often intersertal, with only some small portions having a fluidal displacement of their micro-crystals.

The mineral assemblage is that typical of basaltic products, with phenocrysts of plagioclase (0–57 vol%), clinopyroxene (10–57 vol%), olivine (3–25 vol%), and opaque oxides (3–8 vol%). The pumice and scoriae of Qu deposits have also biotite phenocrysts (up to 10 vol%), whose content decreases from the bottom to the top of the succession. The presence of cumulitic aggregates of clinopyroxene (± plagioclase ± olivine) has been detected especially in the SL formation, with a maximum size of approximately 2400 μm in samples VL18-5 (at the bottom of the volcano-stratigraphic succession).

Plagioclase phenocrysts are generally euhedral, with normal zoning and always twinned. Within the considered volcano-stratigraphic units, only SL presents plagioclase phenocrysts in equilibrium with the surrounding melt. Plagioclase is absent in Quadrara deposits, whereas in the ML scoriae only rare (<5 vol%) relicts of deeply altered (often with sericitization processes) and dissolved plagioclase were found (i.e., xenocrysts). SL deposits also present rare (<5 vol%) xenocrysts or xenocrystic cores, especially in the samples at the bottom of the welded scoriae succession (VL18-5 and SL2 samples; **Figure 5**). Numerous broken plagioclases have been observed within the VL18-5 and SL2 samples, which are two bombs deforming the underlying PDCs dilute deposits (**Figure 5**).

Clinopyroxene crystals are mostly euhedral, ranging between 0.5 and 2 mm in dimensions; they are augitic in composition

and often show several layers of melt inclusions aligned along crystallographic directions. Olivine occurs as euhedral to subhedral phenocrysts, with small grain size (up to 1 mm), and often characterized by iddingsitic post-emplacement alteration. Biotite in Qu Formation is clearly euhedral in the lower white pumice layer, whereas it occurs as antecrysts surrounded by vesiculated colorless glass in the overlying scoriaceous grayish deposits.

PLAGIOCLASE TEXTURAL AND COMPOSITIONAL FEATURES

Despite core-to-rim profiles on plagioclases of SL present a wide compositional interval [An_{43-80} (**Supplementary Material**)], if the whole length of the transects is considered (ca. 16,629 μm; cf. **Supplementary Material**) most of it (ca. 71%, 11,750 μm) show a main composition ranging An_{60-65} (e.g., **Figure 7A**). This feature highlights the occurrence of a population of An_{60-65} plagioclases crystallizing from the same magma reservoir, with the remaining ca. 30% of crystals being perturbed by the magma dynamics occurring prior and during the eruptive event. For SL eruption, these processes, and the related eruptive scenarios, have been studied through the integration of textural investigations and core-to-rim compositional profiles of plagioclase crystals (**Figure 7**). Such analysis led to the identification of four main plagioclase textures, often coexisting in the same crystal, namely (**Figure 7**): (I) Oscillatory Zoning (OZ); (II) Resorbed Cores/Crystals (RC); (III) Envelopes of Resorption (ER); (IV) crystals with alignments of Melt Inclusions (MI). For each sample, textures of all the plagioclase crystals with an apparent length of the c-axis greater than 500 μm (ca. 2000 crystals) were also identified and classified (**Figure 8**).

Plagioclases with oscillatory zoning (OZ) are characterized by small oscillations of the An content in the compositional interval An_{58-65}, as also suggested by the optical features of the crystal. Core-to-rim compositional profiles have evidenced the presence of two different amplitudes of oscillation of the An content, ranging from $\sim\Delta An_{1-3}$ and $\sim\Delta An_{5-7}$ (**Figure 7**). On the whole, the FeO content exhibits a flat, saw-tooth pattern with very narrow variations (up to 0.3 wt%), which remains constant for the whole profile (**Figure 7A**). Phenocrysts with OZ as unique texture are generally rare, and limited to crystals having a maximum length of 600–700 μm. More frequently, this texture represents only a portion of the crystal. The average compositions of OZ segments range in the narrow interval An_{58-65} (cf. **Supplementary Material** and **Figure 7**), resulting in more or less flat profiles interrupted by peaks or bands of more anorthitic compositions related to other textures (**Figure 7**). In some crystals (e.g., VL18-9 Pl 20; **Figure 7A**), although oscillatory zoning presents very little variations (ΔAn_{1-2}), the final transects present a total decrease of ΔAn_8. The frequency of crystals with only OZ in the whole sequence of SL ranges between 5 and 27%, with an apex reached at the base of the welded layer (VL18-6 and VL18-44 samples) and a progressive decrease toward the top of the succession (**Figure 8**).

Resorbed crystals (RC) of plagioclase are characterized by the resorption of the entire crystals or of most of their cores (**Figure 7B**) and re-crystallization of glass. The degree of resorption is very variable, and results in different textures, from small (10–20 μm) pockets of glass (**Figure 7C**) aligned along the *c*-axis direction, to crystals entirely resorbed and deeply fractured (**Figure 7B**). At the end of the event of resorption, plagioclase texture is again OZ, often super-imposed by other growth/dissolution textures. In the residual portions of the crystal, compositional profiles show a marked saw-tooth pattern of the An content at fairly constant FeO, with variation in the order of ΔAn_{7-10} with respect to the normal An_{60-65} range (**Figures 7B,C**). Although in the considered successions this texture presents a wide range of frequency (2–75%; **Figure 8**), it is dominant only within a bomb at the base of the SL sequence (SL-2 sample, up to 75%). Conversely, it is stable at 20–30% in the upper part of the stratigraphic succession (**Figure 8**), and below 10% in the sequence of Mt. Saraceno East.

Plagioclases affected by the development of Envelopes of Resorption (ER) are characterized by levels (up to 80 μm thick) of dusty sieve-textures arranged along the plagioclase growth planes. In correspondence of the micrometric-sized isolated and/or interconnected "pockets" of glass, compositional variations of An and FeO contents are observed (**Figure 7C**). The envelopes of resorption are located at various regions of the crystal, often proportionally to the size of the crystal: in general, the bigger the crystal, the more internal the envelope. Core-to-rim compositional profiles of plagioclase with ER are generally characterized by an increase of ΔAn_{10-12}, which generates An peaks up to An_{72-79}. FeO content could have a concordant increase (up to 0.6 wt%) or remaining fairly constant. In all the considered volcano-stratigraphic successions, the abundance of this texture increases (from 10 to 35%) from the bottom to the top of the deposit (**Figure 8**).

Oscillatory zoning is often super-imposed by alignments of Melt Inclusion (MI) (**Figure 7D**). These layers are characterized by thin (few micrometers) alignments of inclusion of melt, presenting different shapes and arranged along crystallographic directions parallel to the growth planes of the crystal (**Figure 7D**). In correspondence of the alignment of MI a strong increase in the An content (up to ΔAn_{15}) at constant FeO (**Figure 7E**) is observed. When MI alignments and ER textures occur in the same crystal, MI are always in more internal position. Furthermore, more than one envelope of MI can be found within a single crystal (up to 7 in VL18-6 and VL18-51 samples). This texture is by-far the more abundant within all the considered samples (**Figure 8**). In particular, it is dominant in the samples at the bottom of the succession (up to 79%) and tends to decrease its abundance toward the top of the deposit (**Figure 8**).

DISCUSSION

Plagioclase Textures vs. Pre-eruptive Dynamics

During the last 20 years, the technological advancement of microanalytical investigations of volcanic products shed

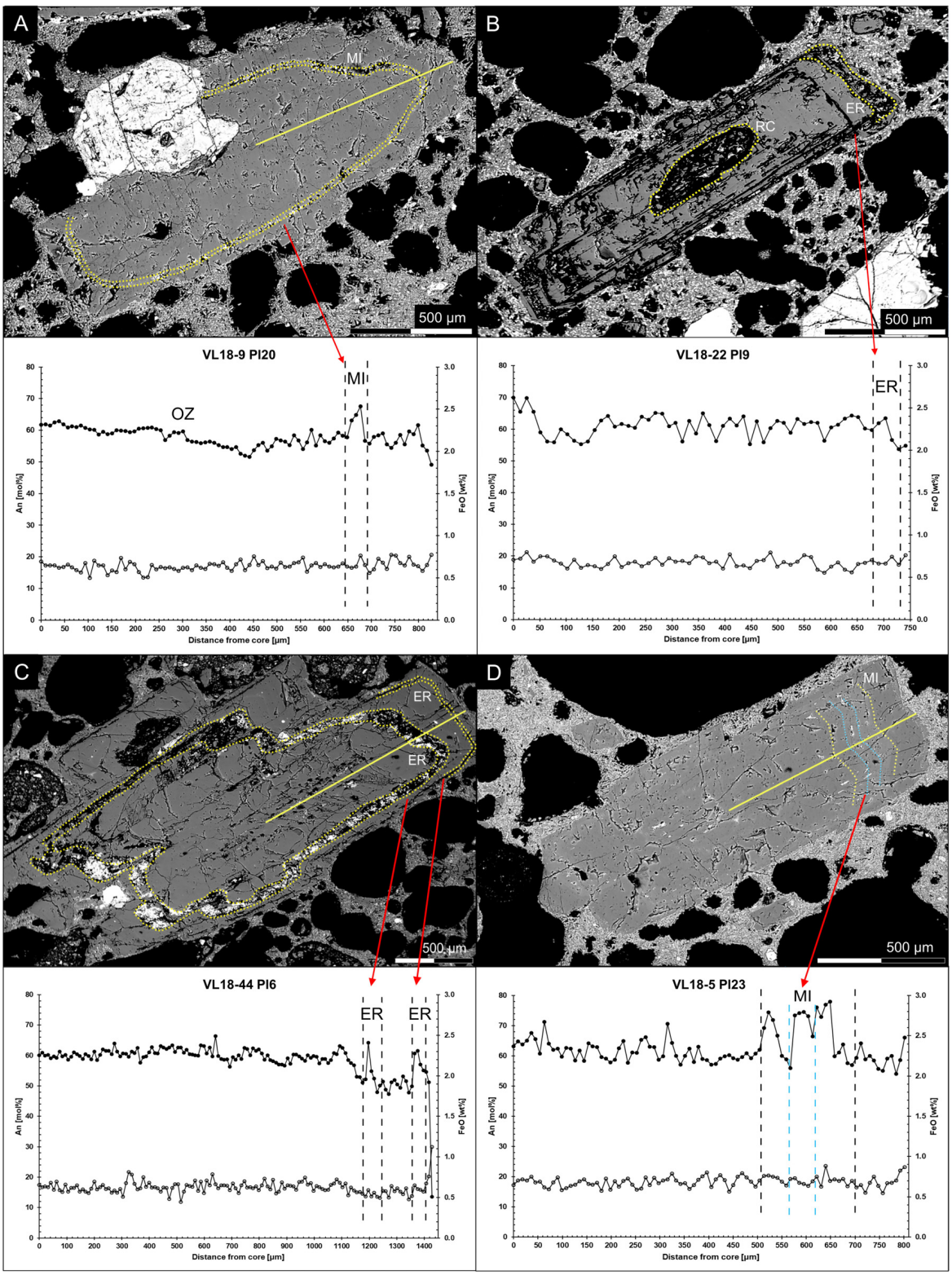

FIGURE 7 | High-contrast and back-scattered images of some representative plagioclase crystals, together with their core-to-rim EMPA/WDS profiles (steps of 5–10 µm). **(A)** Oscillatory zoned (OZ) plagioclase with Melt Inclusion Layers (MIL): in correspondence of the inclusions a peak of $\sim\Delta An_{10}$ is registered, at fairly constant FeO. **(B)** Plagioclase showing a Totally Resorbed Core (TRC) and Enveloped Rims (ER) textures. **(C)** Mildly resorbed Plagioclase crystals (MRC) with a coarsely sieved core, characterized by two layers of ER. **(D)** Plagioclase crystal with three layers of melt inclusions toward the rim of the crystal.

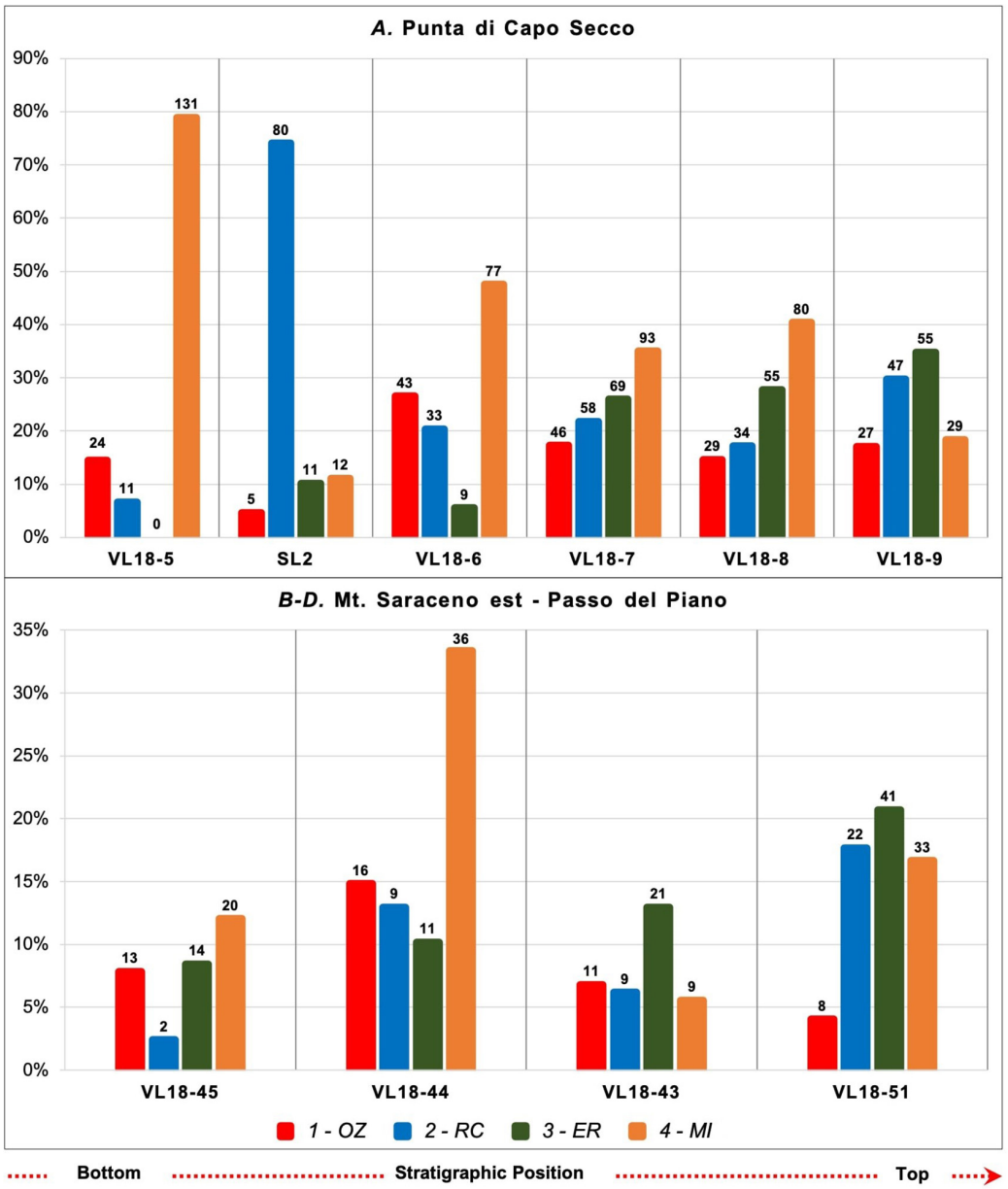

FIGURE 8 | Frequency of phenocrysts (>500 μm) plagioclase textures in the samples of each eruptive unit. Numbers above each histogram represent the number of counted crystals.

light on the way of how magmas store, rise up and interact with other magmas prior and during an eruption (Nelson and Montana, 1992; Pearce, 1994; Singer et al., 1995; Davidson and Tepley, 1997; Clynne, 1999; Streck, 2008; Viccaro et al., 2010, 2016; Kahl et al., 2013; Di Muro et al., 2014; Nicotra et al., 2014, 2018; Ubide and Kamber, 2018; Di Stefano et al., 2020). Indeed, the main phenocrystic phases such as plagioclase, clinopyroxene, olivine, and oxides develop specific textures as a response to any little change of physical and chemical conditions of melts (P-T-X-H_2O) in which they are crystallizing (Anderson, 1984; Kawamoto, 1992; Nelson and Montana, 1992; Pearce, 1994; Singer et al., 1995; Davidson and Tepley, 1997; Clynne, 1999; Tepley et al., 1999; Streck, 2008; Viccaro et al., 2010, 2016; Kahl et al., 2013; Nicotra and Viccaro, 2012a,b; Nicotra et al., 2014, 2018; Ubide and Kamber, 2018). Although a lot of work is still needed, the *routinary* utilization of this microanalytical investigation within the process of analysis of an eruptive event could give an important effort to the assessment and mitigation of volcanic risk. In this paper we use textural and compositional analysis on plagioclase crystals in order to relate the volcanological features observed in the SL welded scoriae at Vulcano island with the pre- and syn-eruptive processes leading

to their formation. Textural and compositional analysis on the welded scoriae of Spiaggia Lunga allowed the identification of four main plagioclase textures (**Figure 7**), namely: (I) Oscillatory Zoning; (II) Resorbed crystals; (III) Envelopes of resorption; (IV) Crystals with alignments of melt inclusion.

Oscillatory zoning (OZ) in plagioclase crystals is characterized by small oscillations of the An content ($<\Delta An_7$) at fairly constant FeO (**Figure 7A**). In the welded scoriae of SL, two different patterns of oscillations have been found ($\sim\Delta An_{2-3}$ and $\sim\Delta An_{5-7}$). The development of this growth texture in plagioclase does not automatically imply significant modifications in chemical and physical parameters of the magmatic system (Allègre et al., 1981; Ortoleva, 1990; Streck, 2008; Nicotra and Viccaro, 2012b). Small amplitude oscillations can be attributed to crystallization kinetics at the crystal/melt interface within a system not affected by significant changes in chemical and physical conditions (cf. Allègre et al., 1981; Ortoleva, 1990; Streck, 2008). Oscillations characterized by larger amplitude (at the same wavelengths) can be instead associated to small changes of the physical and chemical conditions of the magmatic system, but not sufficient to develop major dissolution episodes (Cashman, 1990; Ortoleva, 1990; Pearce and Kolisnik, 1990; Streck, 2008; Viccaro et al., 2010, 2012; Nicotra and Viccaro, 2012a,b; Nicotra et al., 2018). This type of oscillatory zoning is typical of magma reservoirs with small physical (chiefly temperature) and chemical (chiefly H_2O concentrations) gradients, which can trigger fast (but limited) movements of the crystal within the system, and then the development (sometimes) of crenulated surfaces attributed to minor episodes of dissolution (cf. Pearce and Kolisnik, 1990; Singer et al., 1995; Nicotra and Viccaro, 2012a). Summarizing, OZ is a plagioclase texture which can be related to "quiet" conditions of crystallization. The OZ profile of plagioclase VL18-9 Pl20 (in the high part of the SL sequence; **Figures 5**, **7A**), suggests that the magma reservoir in which plagioclase crystallized was not significantly recharged by more primitive magma coming from depth for most of its crystallization history. This is testified by the almost constant decrease from An_{65} to An_{57} in the first half of the profile (**Figure 7A**), with a constant rate ($<\Delta An_{1-2}$). So, for half of its crystallization history, this plagioclase crystallized with compositions ranging An_{57-65} in a magma reservoir which was cooling at fairly constant P-T-X-H_2O conditions.

When magma reservoirs experience major physical perturbations, plagioclase registers the changes of the system through the development of disequilibrium textures, sometimes coupled with compositional changes (Nelson and Montana, 1992; Singer et al., 1995; Davidson and Tepley, 1997; Streck, 2008). Experimental petrology has shown that increased ascent rates reduce the stability field of plagioclase at water-undersaturated and isothermal conditions, provoking its resorption (Nelson and Montana, 1992; Pearce et al., 1987; Streck, 2008). In the welded scoriae of SL, resorbed crystals (RC) of plagioclase could be therefore attributed to a more or less rapid transfer of their host magma within water-undersaturated portions of the plumbing system, and without significant loss of heat during the ascent. Considering that at Vulcano island, for similar whole rock composition, plagioclase would start to crystallize at a depth of 11 km (310–290 MPa; Nicotra et al., 2018), and that the depth of exsolution of H_2O has been calculated at 5 km (130 MPa) by Mandarano et al. (2016), RC plagioclase of SL would have acquired their resorption texture in this pressure interval. Our data do not allow to be more precise about the depth of the mid-crustal reservoir, so we will consider it located between 5 and 11 km of depth. In addition, the observed variability of the degree of dissolution/resorption within the RC plagioclase should be directly proportional to the different ascent rates experienced by the host magma (cf. Nelson and Montana, 1992 and below in the text). The observed coexistence, within the same rock sample of SL, of a wide variability of resorption textures in plagioclase crystals supports the idea of different inputs of fresh magma at different ascent rates from the reservoir located at 11–5 km of depth toward a shallower one. Plagioclase crystals characterized by resorption core surrounded by OZ texture growth (**Figure 7B**) suggest that, prior to the eruption, magma stopped and ponded in the shallow (ca. 5 km b.s.l.) reservoir.

Relationships between the resorption of plagioclase and the ascent rate have been experimentally investigated by Nelson and Montana (1992). These authors empirically related the decompression underwent by magmas at undersaturated-water conditions with the approximate percentages of resorption (i.e., resorption channel and formation of coarse glassy pockets and sieve-textures) observed in plagioclase. If the resorption areas scales with crystal size, considering that: (I) the sizes of SL phenocrysts are about 10–15 times greater than that of the experimental ones, (II) the resorption occurs in an interval of pressure between 300 and 130 MPa, and (III) the approximate area of resorption represents 10–35% of the entire crystal, it could be inferred, using the formulae of Nelson and Montana (1992), that RC texture is acquired within an interval of 2–3 days. Magmas would have rose up between 11 and 5 km with an ascent rate ranging 0.023–0.034 m/sec. Although this range of ascent rates is only indicative, it seems reasonable considering the eruptive scenario of SL and similar results obtained in other tectonic contexts (cf. Browne and Szramek, 2015).

Plagioclase of SL show also Envelopes of Resorption (ER) characterized by layers of dusty sieve-textures (**Figure 7**). Compositional core-to-rim profiles have highlighted that the Envelopes of Resorption correspond to a concordant increase of An and FeO or only an increase of An (ΔAn_{10-12}) at fairly constant FeO. This texture is related to sudden changes in the chemical and physical conditions of the host magma, and is classically associated with the injection of hotter magma, with similar or slightly more basic composition (e.g., Tsuchiyama, 1985; Nakamura and Shimakita, 1998; Streck, 2008; Nicotra and Viccaro, 2012a,b). Therefore, plagioclase with an increase of An and FeO contents in correspondence of the sieve texture envelopes (**Figure 7C**) experienced the injection and mixing of a slightly more basic magma from depth, able to change the FeO content, which typically reflects changes in composition of the system. When the increase of An is accompanied by fairly constant FeO content, the magma that is intruding and mixing with the residing one presents a rather similar composition (as in the case of the SL eruption; cf. **Figure 4**), but its higher volatile elements content and temperature lead to the crystallization of

more An-rich layers of plagioclase: such process is known in literature as cryptic mixing (Nicotra and Viccaro, 2012a; Nicotra et al., 2018; Pizarro et al., 2019). ER textures in plagioclase of SL are usually followed by a OZ "shell," suggesting that the ingress of a new magma into the SL system cannot be considered the trigger of the eruptive event itself. Conversely, the injected magma had enough time to mix with the resident one and be progressively erupted.

One of the most abundant textures within SL plagioclase is that characterized by alignment of Melt Inclusions (MI), super-imposed to oscillatory zoning and presenting a strong increase in the An content (up to ΔAn_{15}) at constant FeO (**Figure 7D**). Present-day literature is still not exhaustive about the mechanisms of entrapment of melt inclusion in plagioclase in such arrangements. This is mainly due to the fact that each inclusion can have different shapes, each with a different petrologic significance (Bennett et al., 2019). In the SL welded scoriae plagioclase, at least two different magma dynamics could be associated to the observed compositional changes in correspondence of MI alignments: (I) a sudden depressurization event in the magma reservoir in which plagioclase were crystallizing (cf. Ustunisik et al., 2014); (II) gas-flushing of the magma chamber where plagioclase were crystallizing, with the gas phase coming from a more deep-seated reservoir. Both processes of decrease of pressure (P) and increase of the water content (P_{H2O}) are able to raise up the An content in the crystallizing envelopes of plagioclase (Yoder and Tilley, 1962; Nielsen et al., 1995; Bennett et al., 2019). We put forward the idea that the An increase, and the relative MI entrapment, could be attributed to a rapid decompression underwent by the magma reservoir where SL plagioclases were crystallizing. Indeed, MI are ever parallel to the growth planes of the crystals, suggesting that such arrangements are related to phases of rapid crystal growth, able to incorporate small drops of melt (Nielsen et al., 1995; Nicotra and Viccaro, 2012b; Cashman and Blundy, 2013; Bennett et al., 2019). The very fact that up to seven parallel alignments of MI have been found in some crystals (VL18-6 and VL18-51 samples), suggests that the magma plumbing system experienced the same number of decompression events. No evidences have been found about gas flushing, usually preceding the upcoming a more deep-seated magma, into the upper crystallizing magma reservoir. In water-undersaturated portions of the plumbing system, the uprising gas phase is able to be re-dissolved into the ponding shallow magma reservoir, finally leading to the selective enrichment of some elements in the encountered portion (e.g., K, Ti, Fe, Rb, Ba, F, Cl). This process, usually called "volatile-induced differentiation" and also observed in some basaltic s.l. volcanic systems (Rittmann, 1962; Burnham, 1979; Caroff et al., 1997; Greenough et al., 1999; de Hoog and van Bergen, 2000; Ferlito et al., 2008; Nicotra et al., 2010; Mazziotti Tagliani et al., 2012; Nicotra and Viccaro, 2012a), is able to produce visible modification in the whole rock composition of magmas, which is also reflected in the crystallizing mineralogical phase. In the plagioclase case, volatile-induced differentiation would have significantly modified the FeO (for effect of the increased fO_2) content in correspondence of the MI alignments, a feature which is never observed in the SL samples. Furthermore, whole rock compositions at SL are clearly not selectively enriched in some elements, but they are concordant with the observed processes of magma rejuvenation.

How a Caldera-Forming Event Can Develop at Vulcano Island

Multidisciplinary investigations, integrating volcanological field survey, geochemistry, mineral chemistry, and petrology, on the ML-SL-Qu welded scoria deposits at Vulcano island have highlighted some common peculiar features which develop during these events, all occurring along the borders of the caldera of "Il Piano." Although the considered volumes for each eruption are very low (up to 0.1 km^3 for the most voluminous eruptive event; De Rosa et al., 1988), their deposits have been able to mantle specific areas of the calderas, giving some hints about their eruptive mechanisms.

Beyond their location along the volcano-tectonic structures of the island, all the considered eruptions are communed by the similarity of their deposits, represented by basic scoriae blankets from poorly to strongly welded. Volcanological survey has also highlighted the presence, at their base, of an alternance of cross-laminated tuff layers, deposited from dilute PDCs, minor and thin fall layers with accretionary lapilli and a high frequency of country crustal rocks (i.e., leuco-monzogabbro; Faraone et al., 1986), features which relate these deposits to a phreatomagmatic event (cf. Schmincke, 2004). These deposits are all strictly related to the successive (in terms of stratigraphic column; **Figure 5**) welded scoriae, as witnessed by the occurrence, in their upper portion, of bombs and blocks which plastically deformed the soft tuffs. These clasts can be either juvenile bombs or also, in the case of SL, pieces of crustal country rocks carried up during the opening of the eruptive fissure. The location of these eruptive events along the rims of "Il Piano" caldera suggests that magmas, after the initial magma-water interaction phase, were able to reach the surface through the newly formed or re-activated ring faults of this caldera (**Figure 9A**).

Once that the initial phases of the caldera-forming eruptions have been outlined, a deeper insight into the geochemical and petrographic features of the erupted magmas suggests distinctive pre- and syn-eruptive dynamics for each of the analyzed welded scoriae deposits.

Deep Magma Ascent at Monte Luccia (ML)

The welded scoriae of ML (48 kyrs; De Astis et al., 1989) cover the northern and central areas of the island, bordering the northernmost subaerial termination of the "Il Piano" caldera. Field survey suggests that they are produced by a low-intensity strombolian-to-hawaiian activity, with some phases of sustained lava fountaining. A small density-driven scoria flow was also emplaced along the northern flanks over the underlying Primordial Vulcano unit. Unfortunately, the lack of plagioclase crystals in equilibrium with the host magmas did not allow information on the pre-eruptive dynamics of this eruption. Nonetheless, this suggests that the ML welded basaltic scoriae derive from a magma coming from a depth higher than those of nucleation of plagioclase. At Vulcano island, this depth has been calculated at ca. 11 km for magmas with shoshonitic

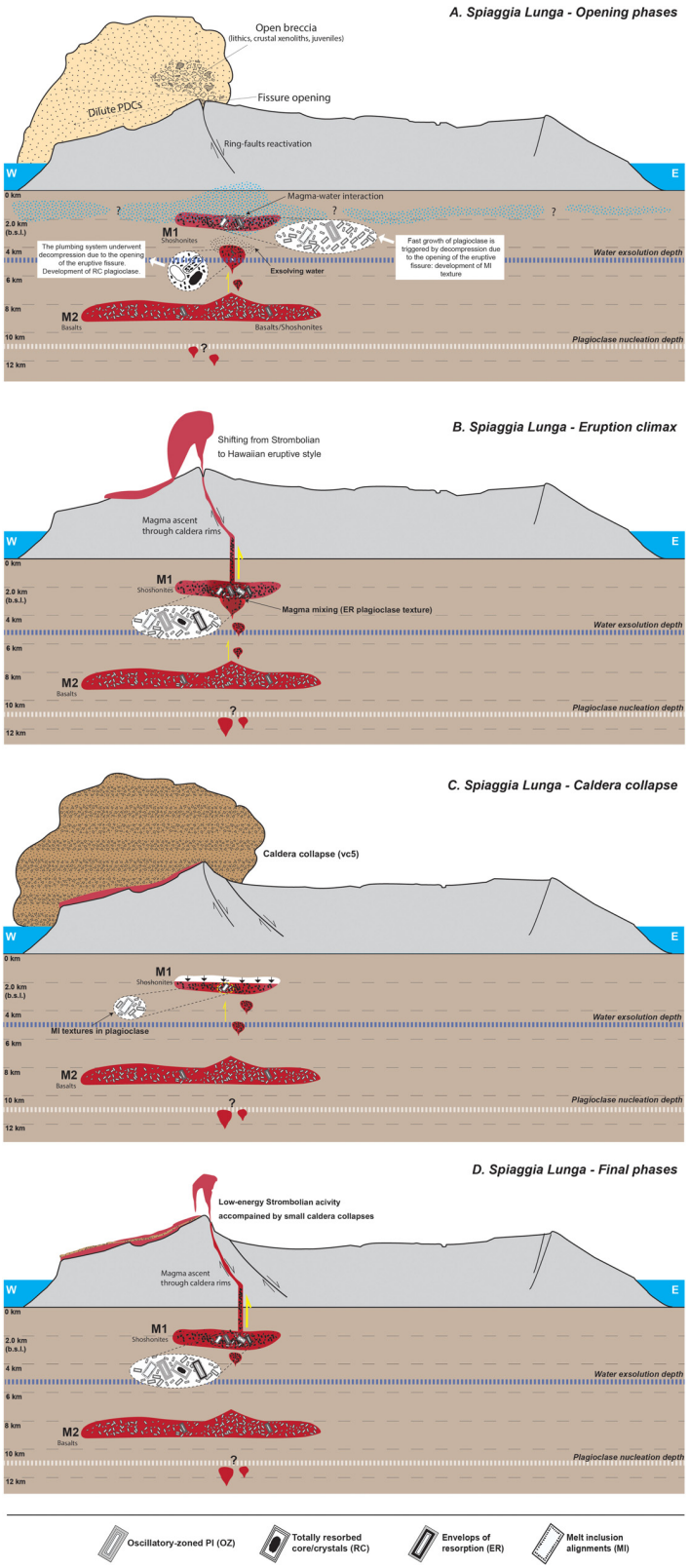

FIGURE 9 | Cartoon showing the different phase of evolution of the Spiaggia Lunga eruption. **(A)** The SL event starts with an phreatomagmatic eruption, where a shallow residing and zoned magma reservoir with shoshonitic/latitic composition interacts with ground- or sea-water. This causes the deposition of the dilute PDCs,

(Continued)

FIGURE 9 | Continued
the formation of the accretionary lapilli, and leads to the opening the eruptive fissure. The magma involved in this initial phase has a shoshonitic composition (M1). The decompression on the system provokes the starting of magma ascent from a water-undersaturated portion of the feeding system (M2, basaltic in composition). During this ascent, RC texture is acquired by plagioclase crystals. **(B)** Onset of the purely magmatic eruption, which starts with a Strombolian eruptive style. The M2 basaltic magma enters into the shallow M1, and efficiently mixes with it. The ingress of a slightly hotter, volatile-rich and more basic magma causes the development of ER texture in plagioclase crystals. The arrival of this new magma at the surface is probably related to the shifting of eruptive style from Strombolian to Hawaiian. The decompression on the system leads to the formation of the MI texture in plagioclase. **(C)** The emptying of the shallow reservoir triggers the collapse of the southern border of the caldera of "Il Piano" (vc5 in De Astis et al., 2013). The deposits of this collapse are evident along the southern flanks of Vulcano island, interlayered within the SL welded scoriae. Such decompression event leads to fast growth of plagioclase and formation of plagioclase with MI textures. **(D)** After the major event, small minor collapses are registered by plagioclase crystals. Eruptive activity turns into strombolian until the end of the eruption.

affinity by means of MELTS simulations (cf. Nicotra et al., 2018). The presence of a deep basaltic/shoshonitic reservoir active throughout the entire eruptive history of Vulcano island has been proposed by several authors, which located it close to the Moho discontinuity (18–21 km b.s.l.; e.g., Zanon et al., 2003; Davì et al., 2009; De Astis et al., 2013; Nicotra et al., 2018). At this stage it is not possible to have more insights about the mechanisms which triggered the ascent of this deep-seated magma. Nonetheless, the similar eruptive dynamics with SL and Qu events (starting with phreatomagmatic eruptions and ascent of magma through the ring-faults of "Il Piano" caldera) can lead to the speculation of a fast magma ascent due to a sudden event of decompression of the plumbing system, similarly to what happened during the SL eruption (see below). However, a hypothesis of eruptive event as response of the ascent of a deep-seated magma (similar to what observed by Nicotra et al., 2018, for the present-day magma at "La Fossa") cannot be ruled out for ML eruption. The area of Monte Luccia (**Figure 1**) was successively cut by the vc4 volcano-tectonic collapse of De Astis et al. (2013).

Spiaggia Lunga as Archetype Caldera-Forming Event at Vulcano

The eruptive event of SL is by far the archetype of the caldera-forming eruptions at Vulcano island, mainly thanks to the higher volume of erupted products (0.1 km^3) and the good exposure of its deposits. In addition, the occurrence of an important and plagioclase-dominated crystal cargo (P.I. 35 vol%) allowed the reconstruction of the pre- and syn-eruptive scenarios of this event. As testified by the geological survey, the first phase of the eruption is represented by a phreatomagmatic phase (**Figure 9A**): at "Punta di Capo Secco" (**Figures 1**, **3**, **5**), the associated dilute PDCs deposits reach 4 m of thickness, which can be related to a medium-energy event. The cross-laminated structure of the deposits is studded, at its top, by a great amount (about 30 vol%) of bomb-sags, made up by juvenile and xenolitic (crustal and volcanic) clasts. They give a direction of provenance of 110°E, which points toward the southwestern-most rim of the "Il Piano" caldera. Among the crustal xenoliths, those with leuco-monzogabbroic composition are the most abundant: given their very shallow position into the crustal portion beneath Vulcano island [ca. 1350 m b.s.l.; Faraone et al. (1986)], these products can be considered as a breccia related to vent opening. We put forward the idea that the magma reservoir activated and involved into these initial stages (M1 in **Figure 9A**) had a shoshonitic composition (**Figure 6** and **Table 1**) and would be located at ca. 2 km b.s.l. of depth, i.e., the depth of provenance of the lithics of leuco-monzogabbros (Faraone et al., 1986). So, the onset of the eruption would be provoked by the interaction of magma residing at ca. 2 km b.sl. and phreatic water, generating a phreatomagmatic event along the pre-existing fractures/faults of the caldera of "Il Piano."

The vent opening-breccia deposits could be related to a second more energetic phase of the SL eruption, in which the eruptive fissure suddenly widened as a consequence of the re-activation of the ring-faults of the "Il Piano" caldera (**Figure 9A**). This volcano-tectonic event would be able to provoke a decompression wave propagating downward in the magmatic plumbing system (**Figure 9A**), as testified by the formation of MI texture on the An_{60-65} plagioclase, which was crystallizing in the shallow shoshonitic M1 reservoir (**Figure 9A**). The rapid decompression event was registered by the plagioclase of the shoshonitic ballistic bombs producing bomb-sags at the top of the dilute PDC deposits (MI = 79% in VL18-5 sample; **Figures 5**, **8**).

The opening of the eruptive fissure would have also provoked the ascent of a more basic magma which was residing in a reservoir, located between 5 km (the exsolution depth of water; cf. Mandarano et al., 2016) and 11 km (plagioclase nucleation depth; Nicotra et al., 2018; M2 in **Figure 9A**). The ascent of magma from the M2 reservoir, at water under-saturated conditions, would have been able to form the RC texture in the plagioclase of SL eruption (RC = 74% in SL2 sample; **Figures 8**, **9A**). The M1 shoshonitic magma then reached the surface with the onset of a low-energy strombolian activity of lava fountaining (**Figure 9B**).

The gradual involvement, within the course of the eruption, of a deeper reservoir (M2) with magmas of more mafic compositions, hotter and richer in volatiles, is testified by numerous factors. Firstly, the evidence of a gradual increase (from 6 to 35%) of dusty sieve-textured plagioclase (ER texture; **Figures 7C**, **8**) from the bottom to the top of the SL stratigraphic column of "Punta Capo di Secco" (**Figure 5**). As previously stated, ER texture is related to the ingress of a slightly more basic, hotter and volatile-rich magma (the M2 in this case) into the system (**Figure 9B**), able to increase both An and FeO content in the plagioclase compositional profiles (**Figure 7**). Secondly, the whole rock compositions at Punta Capo di Secco (**Figure 6C**) outlining that: (i) the SL eruption starts with the emission of shoshonitic products (SiO_2 = 50.3–50.9 wt%, K_2O = 2.84–2.99 wt%; **Figure 6C** and **Table 1**); (ii) the eruption continues without changing the compositions of the magmas up to the main phase of the eruption, which produced the welded central part of the succession (VL18-6, VL18-7, and VL18-8; SiO_2 = 51.4–51.7 wt%, K_2O = 2.73–3.09 wt%; **Figure 6C** and **Table 1**), and (iii) only in

the final stage of the eruption the more basic (basaltic) magma is emitted forming the upper portion of the SL deposits ($SiO_2 < 49$ wt%, $K_2O < 2.8$ wt%; **Figure 6C** and **Table 1**). This suggests that the M2 basaltic magma entered into the system during the course of the eruption and efficiently mixed with the residing M1 (**Figure 9B**), leading to a progressive shifting of whole rock compositions toward more basic terms (**Figure 6C**). Such magma recharge/rejuvenation from the bottom to the top of the succession has been already evidenced by De Rosa et al. (1988). The efficient mixing, and subsequent arrival at the surface of this hotter and more basic magma probably led to the craterization of the eruptive fissure (as proposed by De Rosa et al., 1988) and determined the change of eruptive style from Strombolian to Hawaiian, with an increase of the emission rate witnessed by the extreme welding of the ejected spatter and bombs (**Figure 9B**).

The involvement of the M2 reservoir seems therefore to be related to the occurrence of shallow volcano-tectonic processes, which re-activated, at least, a portion of the plumbing system beneath Vulcano island. This is the opposite of what found by Nicotra et al. (2018) who, analyzing the volcanic activity of the last 1000 years at "La Fossa" and "Vulcanello," have highlighted that the initial trigger of the processes leading to eruptions would be related to the ascent of "fresh" basaltic/shoshonitic magma from the Moho. Nonetheless, the plumbing systems of "La Fossa" and "Il Piano" present very different features, mainly due to a temporal evolution of the systems, which are able to deeply change the dynamics of magma ascent and storage. At "La Fossa," several authors highlighted the occurrence of a polybaric and rather articulated plumbing system, formed by (at least) four different reservoirs located at different depths (cf. Clocchiatti et al., 1994; Zanon et al., 2003; De Astis et al., 2013; Mandarano et al., 2016; Nicotra et al., 2018); each magma reservoir would have a different composition within the range between basalts and rhyolites (cf. Nicotra et al., 2018 and references therein). The "Il Piano" plumbing system is certainly less evolved than "La Fossa" one, at least in terms of the compositions of magmas involved between 48 and 21 kyrs (latites are the most differentiated erupted products). In our reconstruction (**Figure 9**) latitic magmas would be located within the shallow M1 reservoir (2 km b.s.l.), which at "La Fossa" is actually occupied by a degassed rhyolitic magma. The plumbing system of "Il Piano" would be also slightly less articulated, as one of the four reservoirs of "La Fossa" would lack (cf. Clocchiatti et al., 1994; Zanon et al., 2003; De Astis et al., 2013; Mandarano et al., 2016; Nicotra et al., 2018).

Within the stratigraphic column of SL, the main caldera-forming event is testified by 1 m thick layer of chaotic breccia (**Figure 5**), found (with variable thickness) all over the western flank of the "Il Piano" Caldera. The trigger of the caldera collapse is inferred to be the partial emptying of the M1 shallow magma reservoir (**Figure 9C**). Considering the stratigraphic position of the epiclastic deposits occurring at the top of the stratigraphic succession and above the strongly welded deposits (**Figure 5**), we suggest that the caldera collapse can be due to several concurring causes, involving (I) the possible high eruption rate of the "lava-like" Hawaiian phase of the SL eruption and (II) the absence of correlation of this phase with the input of fresh mafic magma from the deeper reservoir. After this major event of collapse along the ring faults of the "Il Piano" caldera, the eruption continued with a decreasing output rate and a shifting toward low-energy strombolian activity (**Figure 9D**). This is testified by the lower degree of welding of the last-emitted products in correspondence of "Capo Secco" (**Figures 3A,D**). During the last phases of SL eruption, small decompression events of fissure opening (**Figure 9D**) are registered by plagioclase crystals, with the development of up to 3 layers of melt inclusions (ever after the envelop of resorption; **Figure 7D**).

Late Re-activation of "Il Piano" Caldera at Quadrara

Quadrara eruptive event (ca. 21 kyrs; Soligo et al., 2000) shows different eruptive dynamics with respect to the Monte Luccia and Spiaggia Lunga eruptions. Although Quadrara's eruption also begins with a phreatomagmatic phase (**Figure 4**), it continues with a thin (0.2–1 m) layer of fall-deriving and biotite-bearing white pumices having latitic compositions (**Figure 6**). The presence of biotite implies the occurrence of an isolated magma reservoir, where the increase of volatile pressure allowed the crystallization of this hydrous mineral phase and where the magma evolved to latitic compositions (**Figure 6**). On the basis of the stratigraphic and physical continuity of the PDC dilute deposits and the overlying pumices, we hypothesize that the onset of the shallow phreatomagmatic activity would have led to the self-activation of the plumbing system. The latitic magma would have been able to rise up through the old ring faults of the Caldera of "Il Piano," giving rise to a typical fall eruption and the deposition of white-to-grayish pumices. The occurrence of a small caldera collapse is here evidenced by a cm-thick epiclastic layer, followed by a grayish-to-black scoria blanket with compositions ranging from latitic to shoshonitic toward the top of the deposit. Such variation could be related, as in the SL eruption, to the retrieval of a basaltic deep magma from the Moho discontinuity, which mixed with the latitic residing one.

CONCLUSION

The integration of a detailed volcanological field survey with geochemistry and textural and compositional investigations on plagioclase crystals allowed to shed light on the pre- and syn-eruptive dynamics of some eruptive events producing welded scoriae associated to small caldera collapses at Vulcano island.

The main points to be remarked are:

I. Between 48 and 21 kyrs the ring-faults and fissures of the caldera of "Il Piano" were the main locus of volcanic activity at Vulcano island. The three most important eruptions of this period [Monte Luccia (ML), Spiaggia Lunga (SL), and Quadrara (Qu)] are characterized by the emplacement of blankets of strongly welded scoriae.
II. All the three considered eruptions started with a phreatomagmatic phase, able to deposit some dilute PDCs and thin fall layers. At the end of this phase, open-breccia deposits and juvenile bombs deformed these underlain still soft deposits.

III. At Monte Luccia, the oldest among the studied eruption, the phreatomagmatic phase and, probably, the widening of the northern caldera faults would have enhanced the ascent of a shoshonitic magma from a reservoir located below the nucleation depth of plagioclase (ca. 11 km at Vulcano). However, a hypothesis of a direct ascent of a deep-seated magma as trigger of the eruptive events cannot be ruled out for ML eruption. This magma rose up directly to the surface, producing Hawaiian to Strombolian eruptive activity.

IV. At Spiaggia Lunga, magmas involved into the phreatomagmatic phase (M1) had a shoshonitic compositions and were residing at 2 km b.s.l., generating plagioclase with OZ texture and An_{60-65} compositions. The decompression due to the volcano-tectonic event formed the MI alignment textures in plagioclase of the M1 reservoir, and caused the ascent of a deep-seated (5–11 km) magma (M2) of basaltic composition. During the ascent, Resorbed Crystal texture formed in plagioclases.

The M2 basaltic magma progressively entered into the M1 reservoir, and gradually mixed with it, as testified the formation of the Envelope of Resorption (ER) texture in plagioclase and by the tendency of whole rock compositions to be more basic from the bottom to the top of the eruptive sequence. The involvement of such more basic magma is also suggested in the shifting of the eruptive style of the eruption, from a low-energy Strombolian to a Hawaiian.

The collapse of the south-western border (vc5 in De Astis et al., 2013) of the "Il Piano" caldera would be therefore the effect of a rapid emptying of the shallow M1 magma reservoir, due to possible high eruption rates during the "lava-like" phase not accompanied by a new input of magma coming from the M2 deep reservoir, which would have been able to re-pressurize the system.

V. At the base of the Quadrara deposits, the occurrence of white latitic pumices layer containing biotite suggests that the eruption started from a shallow, isolated reservoir, where the increase of volatile pressure allowed the crystallization of hydrous phases. A deeper shoshonitic magma was then involved in the last stages on the eruption, forming a scoria level at the top of the sequence.

Results of our study also highlight that the textural and compositional investigations on plagioclase crystals, but also of other phenocrystic phases like pyroxene and olivine, integrated with volcanological s.l. observations and with petrologic monitoring, can contribute to the evaluation and mitigation of volcanic risk through the understanding of how an eruptive scenario will develop.

DATA AVAILABILITY STATEMENT

All datasets generated for this study are included in the article/**Supplementary Material**.

AUTHOR CONTRIBUTIONS

MM executed the textural investigations and compositional profiles of plagioclase crystals, with the scientific support of EN. EN elaborated the resulting data, conceived the model of evolution of the eruptive events. EN wrote the manuscript with the contribution of PD and MM (figures and tables). RD found and managed the funds which allowed this research, and contributed in the elaboration of the model of evolution of the considered eruptive events. All authors performed the volcanological survey and associated rock sampling.

FUNDING

This work was supported by the 2012–2014 DPC-INGV V3 Project grant no. INGV-V3/UR5 (Project Coordinator RD). EN was supported by a *post doc* fellowship from the University of Calabria, title "Dynamics and timescales of magma ascent and storage processes in the Lipari and Vulcano feeding system."

ACKNOWLEDGMENTS

We thank Prof. Mauro Rosi, Dr. Fabio Speranza, Arianna Beatrice Malaguti, and Ilaria Tubia for their help and useful discussions during the field work. We are grateful to Dr. Giancarlo Niceforo and Mariano Davoli for their precious help in the XRF and EMPA analyses, respectively. We also thank the Guest Associate Editor Marc-Antoine Longprè, and two reviewers for their appropriate and useful comments to the first version of the manuscript.

SUPPLEMENTARY MATERIAL

The Supplementary Material for this article can be found online at: https://www.frontiersin.org/articles/10.3389/feart.2020.00223/full#supplementary-material

REFERENCES

Albert, P. G., Giaccio, B., Isaia, R., Costa, A., Niespolo, E. M., Nomade, S., et al. (2019). Evidence for a large-magnitude eruption from Campi Flegrei caldera (Italy) at 29 ka. *Geology* 47, 595–599. doi: 10.1130/g45805.1

Allègre, C. J., Provost, A., and Jaupart, C. (1981). Oscillatory zoning: a pathological case of crystal growth. *Nature* 294, 223–228. doi: 10.1038/294223a0

Andersen, N. L., Singer, B. S., Jicha, B. R., Beard, B. L., Johnson, C. M., and Licciardi, J. M. (2017). Pleistocene to holocene growth of a large upper crustal rhyolitic magma reservoir beneath the active laguna del maule Volcanic field, Central Chile. *J. Petrol.* 58, 85–114. doi: 10.1093/petrology/egx006

Anderson, A. T. (1984). Probable relations between plagioclase zoning and magma dynamics, Fuego volcano, Guatemala. *Am. Mineral.* 69, 660–676.

Annen, C., and Sparks, R. S. (2006). Effects of repetitive emplacement of basaltic intrusions on thermal evolution and melt generation in the crust. *Earth Planet. Sci. Lett.* 203, 937–955. doi: 10.1016/s0012-821x(02)00929-9

Barberi, F., Gandino, A., Gioncada, A., La Torre, P., Sbrana, A., and Zenucchini, C. (1994). The deep structure of the Eolian arc (Filicudi-Panarea-Vulcano sector)

in light of gravity, magnetic and volcanological data. *J. Volcanol. Geoth. Res.* 61, 189–206. doi: 10.1016/0377-0273(94)90003-5

Barberi, F., Innocenti, F., Ferrara, G., Keller, J., and Villar, L. (1974). Evolution of aeolian Arc volcanism (southern Tyrrhenian Sea). *Earth Planet. Sci. Lett.* 21, 269–276. doi: 10.1016/0012-821x(74)90161-7

Bennett, E. N., Lissenberg, C. J., and Cashman, K. V. (2019). The significance of plagioclase textures in mid-ocean ridge basalt (Gakkel Ridge, Arctic Ocean). *Contrib. Mineral. Petr.* 174, 49.

Browne, B., and Szramek, L. (2015). "Rates of magma ascent and storage," in *The Encyclopedia of Volcanoes*, 2nd Edn, eds H. Sigurdsson, B. Houghton, S. McNutt, H. Rymer, and J. Stix (London: Academic Press), 203–214. doi: 10.1016/b978-0-12-385938-9.00009-2

Burnham, C. W. (1979). "Magmas and hydrothermal fluids," in *Geochemistry of Hydrothermal Ore Deposits*, 2nd Edn, ed. H. L. Barnes (Hoboken, NJ: John Wiley and Sons), 71–136.

Caroff, M., Ambrics, C., Maury, R. C., and Cotten, J. (1997). From alkali basalt to phonolite in hand-size samples: vapor-differentiation effects in the Bouzentes lava flow (Cantal, France). *J. Volcanol. Geoth. Res.* 79, 47–61. doi: 10.1016/s0377-0273(97)00023-1

Cashman, K., and Blundy, J. (2013). Petrological cannibalism: the chemical and textural consequences of incremental magma body growth. *Contrib. Mineral. Petr.* 166, 703–729. doi: 10.1007/s00410-013-0895-0

Cashman, K. V. (1990). "Textural constraints on the kinetics of crystallization of igneous rocks," in *Modern Methods of Igneous Petrology: Understanding Magmatic Processes Rev*, Vol. 24, eds J. Nicholls and J. K. Russell (Chantilly, VA: Mineralogical Society of America), 259–314.

Cashman, K. V., and Giordano, G. (2014). Calderas and magma reservoirs. *J. Volcanol. Geoth. Res.* 288, 28–45. doi: 10.1016/j.jvolgeores.2014.09.007

Clocchiatti, R., Del Moro, A., Gioncada, A., Joron, J. L., Mosbach, M., Pinarelli, L., et al. (1994). Assessment of a shallow magmatic system: the 1888–1890 eruption, Vulcano Island, Italy. *Bull. Volcanol.* 56, 466–486. doi: 10.1007/s00445005 0056

Clynne, M. A. (1999). A complex magma mixing origin for rocks erupted in 1915, Lassen Peak, California. *J. Petrol.* 40, 105–132. doi: 10.1093/petroj/40.1.105

Coltelli, M., Del Carlo, P., and Vezzoli, L. (1998). Discovery of a Plinian basaltic eruption of Roman age at Etna volcano, Italy. *Geology* 26, 1095–1098.

Crisci, G. M., De Rosa, R., Esperanca, S., Mazzuoli, R., and Sonnino, M. (1991). Temporal evolution of a three components system: the island of Lipari (Aeolian Arc, southern Italy). *Bull. Volcanol.* 53, 207–221. doi: 10.1007/bf0030 1231

Davì, M., De Rosa, R., Donato, P., Vetere, F., Barca, D., and Cavallo, A. (2009). Magmatic evolution and plumbing system of ring-fault volcanism: the Vulcanello Peninsula (Aeolian Islands, Italy). *Eur. J. Mineral.* 21, 1009–1028. doi: 10.1127/0935-1221/2009/0021-1955

Davì, M., De Rosa, R., and Holtz, F. (2010). Mafic enclaves in the rhyolitic products of Lipari historical eruptions; relationships with the coeval Vulcano magmas (Aeolian Islands, Italy). *Bull. Volcanol* 72, 991–1008. doi: 10.1007/s00445-010-0376-5

Davidson, J. P., and Tepley, F. J. (1997). Recharge in Volcanic systems: evidence from isotope profiles of phenocrysts. *Science* 275, 826–829. doi: 10.1126/science.275.5301.826

De Astis, G., Frazzetta, G., and La Volpe, L. (1989). I depositi di riempimento della caldera del Piano ed i depositi della Lentia. *Bollett. G. N. V.* 2, 763–778.

De Astis, G., La Volpe, L., Peccerillo, A., and Civetta, L. (1997). Volcanological and petrological evolution of Vulcano Island (Aeolian Arc, southern Tyrrhenian Sea). *J. Geophys. Res.* 102, 8021–8050. doi: 10.1029/96jb03735

De Astis, G., Lucchi, F., Dellino, P., La Volpe, L., Tranne, C. A., Frezzotti, M. L., et al. (2013). "Geology, volcanic history and petrology of Vulcano (central Aeolian archipelago)," in *The Aeolian Islands Volcanoes*, Vol. 37, eds F. Lucchi, A. Peccerillo, J. Keller, C. A. Tranne, and P. L. Rossi (London: Geological Society of London), 281–349. doi: 10.1144/m37.11

de Hoog, J., and van Bergen, M. (2000). Volatile-induced transport of HFSE, REE, Th and U in arc magmas: evidence from zirconolite-bearing vesicles in potassic lavas of Lewotolo volcano (Indonesia). *Contrib. Mineral. Petr.* 139, 485–502. doi: 10.1007/s004100000146

De Ritis, R., Ravat, D., Ventura, G., and Chiappini, M. (2013). Curie isotherm depth from aeromagnetic data constraining shallow heat source depths in the central Aeolian Ridge (Southern Tyrrhenian Sea, Italy). *Bull. Volcanol.* 75:710.

De Rosa, R., Guillou, H., Mazzuoli, R., and Ventura, G. (2003). New unspiked K-Ar ages of volcanic rocks of the central and western sector of the Aeolian Islands: reconstruction of the volcanic stages. *J. Volcanol. Geoth. Res.* 120, 161–178. doi: 10.1016/s0377-0273(02)00369-4

De Rosa, R., Mazzuoli, R., Frazzetta, G., and La Volpe, L. (1988). The spiaggia lunga scoriae deposits: an example of fissural type eruption at Vulcano (Aeolian Islands, Italy). *Rend. Soc. Ital. Mineral. Petrol.* 43, 1059–1068.

Del Moro, A., Gioncada, A., Pinarelli, L., Sbrana, A., and Joron, J. L. (1998). Sr, Nd, and Pb isotope evidence for open system evolution at Vulcano, Aeolian Arc, Italy. *Lithos* 43, 81–106. doi: 10.1016/s0024-4937(98)00008-5

Di Muro, A., Métrich, N., Vergani, D., Rosi, M., Armienti, P., Fougereox, T., et al. (2014). The shallow plumbing system of Piton de la Fournaise volcano (La Réunion Island, Indian Ocean) revealed by the major 2007 caldera forming eruption. *J. Petrol.* 55, 1287–1315. doi: 10.1093/petrology/egu025

Di Stefano, F., Mollo, S., Ubide, T., Petrone, C. M., Caulfield, J., Scarlato, P., et al. (2020). Mush cannibalism and disruption recorded by clinopyroxene phenocrysts at Stromboli volcano: new insights from recent 2003–2017 activity. *Lithos* 360–361:105440. doi: 10.1016/j.lithos.2020.105440

Ellam, R. M., Hawkesworth, C. J., Menzies, M. A., and Rogers, N. W. (1989). The volcanism of southern Italy: role of subduction and the relationships between potassic and sodic alkaline magmatism. *J. Geophys. Res.* 94, 4589–4601. doi: 10.1029/jb094ib04p04589

Esperança, S., Crisci, G. M., De Rosa, R., and Mazzuoli, R. (1992). The role of the crust in the magmatic evolution of the Island of Lipari (Aeolian Islands, Italy). *Contrib. Mineral. Petr.* 112, 450–462. doi: 10.1007/bf00310777

Fabbro, G. N., Druitt, T. H., and Scaillet, S. (2013). Evolution of the crustal magma plumbing system during the build-up to the 22-ka caldera-forming eruption of Santorini (Greece). *Bull. Volcanol.* 75, 1–22.

Faraone, D., Silvano, A., and Verdiani, G. (1986). The monzogabbroic intrusion in the island of Vulcano, Aeolian Archipelago, Italy. *Bull. Volcanol.* 48, 299–307. doi: 10.1007/bf01081758

Ferlito, C., Viccaro, M., and Cristofolini, R. (2008). Volatile-induced differentiation in the plumbing system of Mt. Etna volcano (Italy): evidence from glass and tephra of the 2001 eruption. *Bull. Volcanol.* 70, 455–473. doi: 10.1007/s00445-007-0149-y

Fontaine, F. R., Roult, G., Michon, L., Barruol, G., and Di Muro, A. (2014). The 2007 eruptions and caldera collapse of the Piton de la Fournaise volcano (La Réunion Island) from tilt analysis at a single very broadband seismic station. *Geophys. Res. Lett.* 41, 2803–2811. doi: 10.1002/2014gl059691

Frezzotti, M. L., Peccerillo, A., Zanon, V., and Nikogosian, I. (2004). Silica-rich melts in quartz xenoliths from Vulcano Island and their bearing on processes of crustal anatexis and crust–magma interaction beneath the Aeolian Arc, Southern Italy. *J. Petrol.* 45, 3–26. doi: 10.1093/petrology/egg080

Gasparini, C., Iannaccone, G., Scandone, P., and Scarpa, R. (1982). Seismotectonics of the Calabrian Arc. *Tectonophysics* 82, 267–286. doi: 10.1016/0040-1951(82)90163-9

Gioncada, A., and Sbrana, A. (1991). La Fossa Caldera, Vulcano: inferences from deep drillings. *Acta Vulcanol.* 1, 115–126.

Greenough, J., Lee, C., and Fryer, B. (1999). Evidence for volatile-influenced differentiation in a layered alkali basalt flow, Penghu Islands, Taiwan. *Bull. Volcanol.* 60, 412–424. doi: 10.1007/s004450050241

Gudmundsson, A. (2012). Magma chambers: formation, local stresses, excess pressures, and compartments. *J. Volcanol. Geoth. Res.* 237-238, 19–41. doi: 10.1016/j.jvolgeores.2012.05.015

Gvirtzman, Z., and Nur, A. (1999). The formation of Mount Etna as the consequence of slab rollback. *Nature* 401, 782–785. doi: 10.1038/44555

Harpp, K. S., and Geist, D. J. (2018). The Evolution of Galápagos Volcanoes: an alternative prospective. *Front. Earth Sci.* 6:50. doi: 10.3389/feart.2018.00050

Jellinek, A., and de Paolo, D. (2003). A model for the origin of large silicic magma chambers: precursors of caldera-forming eruptions. *Bull. Volcanol.* 65, 363–381. doi: 10.1007/s00445-003-0277-y

Kahl, M., Chakraborty, S., Costa, F., Pompilio, M., Liuzzo, M., and Viccaro, M. (2013). Compositionally zoned crystals and real-time degassing data reveal changes in magma transfer dynamics during the 2006 summit eruptive episodes of Mt. Etna. *Bull. Volcanol.* 75:692.

Kawamoto, T. (1992). Dusty and honeycomb plagioclase: indicators of processes in the Uchino stratified magma chamber, Izu Peninsula, Japan. *J. Volcanol. Geoth. Res.* 49, 191–208. doi: 10.1016/0377-0273(92)90014-5

Keller, J. (1980). The island of Vulcano. *Rend. della Soc. Ital. di Mineral. Petrogr.* 3, 369–414.

Kennedy, B., Holohan, E. P., Stix, J., Gravley, D. M., Davidson, J. R. J., and Cole, J. W. (2018). Magma plumbing beneath collapse caldera volcanic systems. *Earth Sci. Rev.* 177, 404–424. doi: 10.1016/j.earscirev.2017.12.002

Mandarano, M., Paonita, A., Martelli, M., Viccaro, M., Nicotra, E., and Millar, I. L. (2016). Revealing magma degassing below closed-conduit active volcanoes: geochemical features of volcanic rocks versus fumarolic fluids at Vulcano (Aeolian Islands, Italy). *Lithos* 248-251, 272–287. doi: 10.1016/j.lithos.2016.01.026

Marsh, B. D. (1996). Solidification fronts and magmatic evolution. *Mineral. Mag.* 60, 5–40. doi: 10.1180/minmag.1996.060.398.03

Mazziotti Tagliani, S., Nicotra, E., Viccaro, M., and Gianfagna, A. (2012). Halogen-dominant mineralization at Mt. Calvario dome (Mt. Etna) as a response of volatile flushing into the magma plumbing system. *Miner. Petrol.* 106, 89–105. doi: 10.1007/s00710-012-0215-9

Nakamura, M., and Shimakita, S. (1998). Dissolution origin and syn-entrapment compositional changes of melt inclusions in plagioclase. *Earth Planet. Sci. Lett.* 161, 119–133. doi: 10.1016/s0012-821x(98)00144-7

Nelson, S. T., and Montana, A. (1992). Sieve-textured plagioclase in volcanic rocks produced by rapid decompression. *Am. Mineral.* 77, 1242–1249.

Nicotra, E., Giuffrida, M., Viccaro, M., Donato, P., D'Oriano, C., Paonita, A., et al. (2018). Timescales of pre-eruptive magmatic processes at Vulcano (Aeolian Islands, Italy) during the last 1000 years. *Lithos* 316-317, 347–365. doi: 10.1016/j.lithos.2018.07.028

Nicotra, E., and Viccaro, M. (2012a). Transient uprise of gas and gas-rich magma batches fed the pulsating behaviour of the 2006 eruptive episodes at Mt. Etna volcano. *J. Volcanol. Geoth. Res.* 22, 102–118. doi: 10.1016/j.jvolgeores.2012.03.004

Nicotra, E., and Viccaro, M. (2012b). Unusual magma storage conditions at Mt. Etna (Southern Italy) as evidenced by plagioclase megacryst-bearing lavas: implications for the plumbing system geometry and summit caldera collapse. *Bull. Volcanol.* 74, 795–815. doi: 10.1007/s00445-011-0566-9

Nicotra, E., Viccaro, M., De Rosa, R., and Sapienza, M. (2014). Volcanological evolution of the Rivi-Capo Volcanic complex at Salina, Aeolian Islands: magma storage processes and ascent dynamics. *Bull. Volcanol.* 76, 840–864.

Nicotra, E., Viccaro, M., Ferlito, C., and Cristofolini, R. (2010). Influx of volatiles into shallow reservoirs at Mt. Etna volcano (Italy) responsible for halogen-rich magmas. *Eur. J. Mineral.* 22, 121–138. doi: 10.1127/0935-1221/2010/0022-1991

Nielsen, R. L., Crum, J., Bourgeois, R., Hascall, K., Forsythe, L. M., Fisk, M. R., et al. (1995). Melt inclusions in high−an plagioclase from the Gorda Ridge: an example of the local diversity of MORB parent magmas. *Contrib. Mineral. Petr.* 122, 34–50. doi: 10.1007/s004100050111

Ortoleva, P. J. (1990). Role of attachment kinetic feedback in the oscillatory zoning of crystal grown from melts. *Earth Sci. Rev.* 29, 3–8. doi: 10.1016/0012-8252(90)90023-o

Pearce, T. H. (1994). "Recent work on oscillatory zoning in plagioclase," in *Feldspars and Their Reactions*, ed. I. Parsons (Dordrecht: Kluwer Academic Publisher), 313–349. doi: 10.1007/978-94-011-1106-5_8

Pearce, T. H., and Kolisnik, A. M. (1990). Observations of plagioclase zoning using interference imaging. *Earth Sci. Rev.* 29, 9–26. doi: 10.1016/0012-8252(0)90024-p

Pearce, T. H., Russel, J. K., and Wolfson, I. (1987). Laser-interference and Nomarski interference imaging of zoning profiles in plagioclase phenocrysts from the May 18, 1980, eruption of Mount St. Helens, Washington. *Am. Mineral.* 72, 1131–1143.

Peccerillo, A., Donati, C., Santo, A. P., Orlando, A., Yirgu, G., and Ayalew, D. (2007). Petrogenesis of silicic peralkaline rocks in the Ethiopian rift: geochemical evidence and volcanological implications. *J. Afr. Earth Sci.* 48, 161–173. doi: 10.1016/j.jafrearsci.2006.06.010

Peccerillo, A., and Frezzotti, M. L. (2015). Magmatism, mantle evolution and geodynamics at the converging plate margins of Italy. *J. Geol. Soc. Lond.* 172, 407–427. doi: 10.1144/jgs2014-085

Peccerillo, A., and Taylor, S. R. (1976). Geochemistry of eocene calc-alkaline volcanic rocks from the Kastamonu Area, Northern Turkey. *Contrib. Mineral. Petr.* 58, 63–81. doi: 10.1007/bf00384745

Pizarro, C., Parada, M. A., Contreras, C., and Morgado, E. (2019). Cryptic magma recharge associated with the most voluminous 20th century eruptions (1921, 1948 and 1971) at Villarrica Volcano. *J. Volcanol. Geoth. Res.* 384, 48–63. doi: 10.1016/j.jvolgeores.2019.07.001

Rittmann, A. (1962). *Volcanoes and Their Activity*. New York, NY: John Wiley & Sons, 305.

Ruch, J., Vezzoli, L., De Rosa, R., Di Lorenzo, R., and Acocella, V. (2016). Magmatic control along a strike-slip volcanic arc: the central Aeolian arc (Italy). *Tectonics* 35, 407–424. doi: 10.1002/2015tc004060

Sainz-Maza Aparicio, S., Martí, J., Montesinos, F. G., Borreguero Gómez, A., Pereda de Pablo, J., Vaquero Fernández, P., et al. (2019). Gravimetric study of the shallow basaltic plumbing system of Tenerife, Canary Islands. *Phys. Earth Planet. Inter.* 297, 106319. doi: 10.1016/j.pepi.2019.106319

Schmincke, H. (2004). *Volcanism*. Berlin: Springer-Verlag, 324.

Singer, B. S., Dungan, M. A., and Layne, G. D. (1995). Textures and Sr, Ba, Mg, Fe, K and Ti compositional profiles in volcanic plagioclase: clues to the dynamics of calc-alkaline magma chamber. *Am. Mineral.* 80, 776–798. doi: 10.2138/am-1995-7-815

Soligo, M., De Astis, G., Delitala, M. C., La Volpe, L., Taddeucci, A., and Tuccimei, P. (2000). Uranium-series disequilibria in the products from Vulcano Island (Sicily, Italy): isotopic chronology and magmatological implications. *Acta Vulcanol.* 12, 49–59.

Streck, M. J. (2008). "Mineral textures and zoning as evidence for open system processes," in *Minerals, Inclusions and Volcanic Processes. Reviews in Mineralogy and Geochemistry*, Vol. 69, eds K. D. Putirka and F. J. III Tepley (Chantilly, VA: Mineralogical Society of America), 595–622. doi: 10.1515/9781501508486-016

Sun, S. S., and McDonough, W. F. (1989). "Chemical and isotopic systematics of oceanic basalts: implications for mantle composition and processes," in *Magmatism in Ocean Basins*, Vol. 42, eds A. D. Saunders and M. J. Norry (London: Geological Society of London), 313–345. doi: 10.1144/gsl.sp.1989.042.01.19

Tepley, F. J. III, Davidson, J. P., and Clynne, M. A. (1999). Magmatic interactions as recorded in plagioclase phenocrysts of Chaos Crags, Lasses volcanic center, California. *J. Petrol.* 40, 787–806. doi: 10.1093/petroj/40.5.787

Tsuchiyama, A. (1985). Dissolution kinetics of plagioclase in the melt of the system diopside-albite-anorthite, and the origin of dusty plagioclase in andesites. *Contrib. Mineral. Petr.* 89, 1–16. doi: 10.1007/bf01177585

Ubide, T., and Kamber, B. S. (2018). Volcanic crystals as time capsules of eruption history. *Nat. Commun.* 9:326.

Ustunisik, G., Kilinc, A., and Nielsen, R. L. (2014). New insights into the processes controlling compositional zoning in plagioclase. *Lithos* 200–201, 80–93. doi: 10.1016/j.lithos.2014.03.021

Ventura, G. (2013). "Kinematics of the Aeolian volcanism (Southern Tyrrhenian Sea) from geophysical and geological data," in *The Aeolian Islands Volcanoes*, Vol. 37, eds F. Lucchi, A. Peccerillo, J. Keller, C. A. Tranne, and P. L. Rossi (London: Geological Society of London), 3–11. doi: 10.1144/m37.2

Ventura, G., Vilardo, G., and Bruno, P. P. (1999). The role of flank collapse in modifying the shallow plumbing system of volcanoes: an example from Somma–Vesuvius, Italy. *Geophys. Res. Lett.* 26, 3681–3684. doi: 10.1029/1999gl005404

Viccaro, M., Barca, D., Bohrson, W. A., D'Oriano, C., Giuffrida, M., Nicotra, E., et al. (2016). Crystal residence time from trace element zoning in plagioclase reveal changes in magma transfer dynamics at Mt. Etna during the last 400 years. *Lithos* 248–251, 309–323. doi: 10.1016/j.lithos.2016.02.004

Viccaro, M., Giacomoni, P. P., Ferlito, C., and Cristofolini, R. (2010). Dynamics of magma supply at Mt. Etna volcano (Southern Italy) as revealed by textural and compositional features of plagioclase phenocryst. *Lithos* 116, 77–91. doi: 10.1016/j.lithos.2009.12.012

Viccaro, M., Giuffrida, M., Nicotra, E., and Ozerov, A. Y. (2012). Magma storage, ascent and recharge history prior to the 1991 eruption at Avachinsky Volcano, Kamchatka, Russia: inferences on the plumbing system geometry. *Lithos* 140–141, 11–24. doi: 10.1016/j.lithos.2012.01.019

Wang, C. Y., Hwang, W. T., and Shi, Y. (1989). Thermal evolution of a rift basin: the Tyrrhenian Sea. *J. Geophys. Res.* 94, 3991–4006. doi: 10.1029/jb094ib04p03991

Yoder, H. S., and Tilley, C. E. (1962). Origin of basalt magmas: an experimental study of natural and synthetic rock systems. *J. Petrol.* 3, 342–532. doi: 10.1093/petrology/3.3.342

Zanella, E., De Astis, G., and Lanza, R. (2001). Paleomagnetism of welded, pyroclastic-fall scoriae at Vulcano, Aeolian Archipelago. *J. Volcanol. Geoth. Res.* 107, 71–86. doi: 10.1016/s0377-0273(00)00298-5

Zanon, V., Frezzotti, M. L., and Peccerillo, A. (2003). Magmatic feeding system and crustal magma accumulation beneath Vulcano Island (Italy): evidence from CO_2 fluid inclusions in quartz xenoliths. *J. Geophys. Res.* 108:2298. doi: 10.1029/2002JB002140

Conflict of Interest: The authors declare that the research was conducted in the absence of any commercial or financial relationships that could be construed as a potential conflict of interest.